https://doi.org/10.5194/egusphere-2026-3536
Preprint. Discussion started: 6 July 2026

Smoke transport and potential impacts from all observed pyroCb events in North America during 2013-2023

Rubel Chandra Das[1], Jean-Paul Vernier[1,2,5], Amit Kumar Pandit[1], David A. Peterson[3], Michael D. Fromm[4], George Kablick[4], Nicolas Dumelié[5], Lilian Joly [5], and James Flaten[6]

[1]National Institute of Aerospace, Hampton, VA, USA

[2]NASA Langley Research Center, Hampton, VA, USA

[3]Naval Research Laboratory, Monterey, California, USA

[4]Naval Research Laboratory, Washington, DC, USA

[5]Université de Reims Champagne-Ardenne, GSMA UMR CNRS 7331, France

[6]Aerospace Engineering and Mechanics Department, University of Minnesota, Minneapolis, MN, USA

Correspondence to: Rubel Chandra Das (rubel.das@nianet.org)

Abstract. Pyrocumulonimbus (pyroCb) events provide an efficient pathway for wildfire smoke and combustion products to enter the Upper Troposphere and Lower Stratosphere (UTLS), where they are transported far from their source regions and perturb atmospheric composition, radiation, and dynamics. Although there are individual case studies, their cumulative transport behaviour over decadal time scales remains insufficiently characterized. Here, we investigate the short-, mid-, and long-range transport pathways, seasonal and regional variability, vertical structure, and residence characteristics of smoke from all observed North American pyroCbs during 2013–2023 using the Langley Trajectory Model, evaluated against satellite observations. Results show that smoke transport is influenced by source region, season, injection layer, and the evolving synoptic-scale circulation. Summer accounts for the majority of events, while Canadian pyroCbs occur more frequently than pyroCbs in the United States and dominate much of the UTLS and long-range trans-Atlantic transport. Canadian smoke is often transported along midlatitude pathways toward Europe, whereas U.S. pyroCbs more strongly contribute to lower-latitude short- and mid-range transport and to tropical transport pathways. Short- and mid-range tropospheric transport reveals persistent free- and upper-tropospheric downstream convergence regions, indicating areas where smoke may repeatedly influence clouds, radiation, and weather-relevant conditions. In contrast, UTLS and stratospheric transport pathways exhibit faster and longer-range transport, including recurrent midlatitude, tropical, and potential cross-hemispheric pathways. This study provides a decadal transport framework for interpreting how smoke injected by North American pyroCbs is subsequently redistributed. The results help connect pyroCb smoke with observed smoke signatures and atmospheric impacts, while also supporting future model evaluation and mission planning.

1 Introduction

Intense wildfires in recent years have produced fire-driven deep convection ranging from pyrocumulus (pyroCu) to pyrocumulonimbus (pyroCb), impacting the full depth of the atmosphere from the boundary layer to the stratosphere (Fromm et al., 2022, Peterson et al., 2025a). Extreme wildfire events, such as the 2023 Canadian fires (Khaykin et al., 2025, Jain et al., 2024), are happening at higher frequency due to multiple factors including increased large scale climate modulation, changes in vegetations, heat waves, global warming, and also closely linked to the threefold increase in Arctic warming and land–sea thermal contrast (Li et al., 2025). Smoke plumes injected to high altitudes by wildfires are a critical hazard in several regions worldwide, especially in North America. Their accumulated radiative impacts match medium-size volcanic scale plumes. For example, the smoke aerosol mass injected into the stratosphere by pyroCb activity during the Pacific Northwest Event (PNE) on 12 August 2017, was comparable to a moderate volcanic eruption (Peterson et al., 2018). The study of stratospheric smoke injection from wildfires is relatively new, compared to a long history of volcanic study, starting in the late 1990s and early 2000s (Fromm et al 2005).

Extreme wildfires do not only impact the boundary layer but create pyroCb which can modify stratospheric composition (e.g., UTLS, stratosphere where they can persist longer, weeks to months) and have chemical-radiative-dynamical impacts (Fromm et al., 2010, Das et al., 2021, Katich et al., 2023, Bernath et al., 2022, Solomon et al., 2022). The long residence time of pyroCb smoke makes it possible to have global and cross-hemispheric transport and persistent radiative-dynamical impacts. Although extreme singular events such as the 2017 PNE are less frequent, a succession of smaller-scale pyroCbs within a single season can cumulatively inject an aerosol mass comparable to that of mega-events like the 2019/2020 Australian Black Summer (Peterson et al., 2021; Katich et al., 2023). However, unlike the Australian event which involved subsequent self-lofting of smoke deep into the mid-stratosphere (Khaykin et al., 2020, Kablick et al., 2020), smoke injected by these smaller-scale clusters typically resides within the upper troposphere and lowermost stratosphere, limiting the longevity of the plume (Khaykin et al., 2025; Zhang et al., 2024).

The transport of pyroCb smoke from the injection region into the Upper Troposphere and Lower Stratosphere (UTLS) is governed by the interplay between mesoscale dynamics and large-scale atmospheric circulation (Fromm et al., 2010; Peterson et al., 2018). Following the initial convective injection, smoke plumes are rapidly advected zonally by the subtropical and polar jet streams, typically traversing intercontinental distances within days (Khaykin et al., 2018). While the primary injection is driven by the fire-induced convection itself, secondary transport into the stratosphere can occur through synoptic-scale mixing processes, such as tropopause folding and warm conveyor belts, particularly within jet-front systems (Khaykin et al., 2025). Once established in the stratosphere, the residence time and global distribution of the aerosol burden are controlled by the slower Brewer–Dobson circulation and isentropic wave-mixing, processes which redistribute the smoke meridionally over timescales of weeks to months (Butchart, 2014; Kloss et al., 2019). In the immediate aftermath of an event, the plume structure is highly sensitive to the local synoptic environment; for instance, the spread of smoke from the Chuckegg Creek fire (Alberta, Canada, near 58.1°N and 117.1°W, on June 17th, 2019, at 20:00 UTC) was shaped by the

https://doi.org/10.5194/egusphere-2026-3536
Preprint. Discussion started: 6 July 2026

interaction between a blocking high-pressure ridge and a downstream cyclonic system, organizing the aerosol into distinct layers aligned with the upper-level flow (Osborne et al. 2022). Over a longer period of time, transport can involve cross-latitude pathways that connect midlatitude injection regions to the subtropics and tropics, for example, the 2017 PNE event shows that part of the plume was transported through the interaction with the Asian monsoon circulation (Kloss et al 2019). These pathways matter because they determine which regions experience persistent aerosol anomalies in the stratosphere, UTLS, even troposphere, and where the radiative, chemical effects may accumulate.

PyroCb smoke has emerged as a significant and newly recognized source of stratospheric aerosols with important consequences for ozone chemistry. Stratospheric smoke particles facilitate heterogeneous reactions that can perturb reactive nitrogen and halogen cycles, ultimately leading to reductions in stratospheric ozone, particularly when the smoke persists for extended periods (Solomon et al., 2022). Recent observations reveal that major pyroCb events have contributed to measurable ozone losses over the midlatitudes, with studies documenting that intense smoke injections, such as those following the 2019–2020 Australian fires, resulted in substantial stratospheric ozone depletion and may delay ozone recovery (Bernath et al., 2022; Solomon et al., 2022). These findings underscore the need for continued study of pyroCb smoke impacts on the stratospheric ozone layer using in situ measurements, satellite observations, and atmospheric modelling.

In addition, pyroCb smoke-driven heating can alter local temperature and wind fields that can give feedback on the local circulation and can modify the subsequent transport (e.g., Yu et al., 2019; Allen et al., 2020). These coupled chemical-dynamical pathways can influence the UTLS environment far downstream of the source region (Peterson et al., 2018). In some extreme cases, radiative heating (leads to self-lofting of the smoke) can couple with dynamics creating smoke-charged vortices (coherent structures, Smoke with Induced Rotation and Lofting (SWIRL)) that can persist weeks to months, especially in the stratosphere, travel long distances resisting any descent (Allen et al., 2020; Khaykin et al., 2020). These processes link the transport, vertical evolution, aerosol absorption, and how it can affect vertical transport as well as horizontal transport (Katich et al., 2023; Solomon et al., 2022).

While significant focus has been placed on large pyroCb events (e.g., PNE 2017), key gaps remain related to transport focused questions from a climatological point of view, which accounts all small and large pyroCbs. Since individual smaller events are difficult to quantify with their impacts or transport pathways, looking at them as a group to estimate their overall influences gets more meaningful and interpretable. What is needed are transport pathways that (i) treat pyroCb smoke a population of events with strong variability, (ii) quantify their typical pathways, seasonality, regionality, vertical structure, residence time, (iii) connect the Lagrangian findings with what exactly satellite observes in terms of aerosol (e.g., OMPS-AI) and trace gas signals (e.g., MLS-CO). This study addresses these needs focusing on the North American pyroCb smoke from complementary point of view. We use a Lagrangian trajectory framework to map likely pathways and quantify how plume influence evolves in space and time, emphasizing both immediate downstream transport relevant for short-range impacts and the longer-range dispersal relevant for tropospheric, UTLS, and stratospheric residence. To build confidence and physical interpretation, we evaluate the transport pattern against multiple independent satellite proxies that capture different parts of

https://doi.org/10.5194/egusphere-2026-3536
Preprint. Discussion started: 6 July 2026

the smoke systems (e.g., MLS-CO, OMPS-AI, CALIOP/CALIPSO backscatter, and depolarization vertical profiles). A major goal of the current studies is not only providing the qualitative tracking of the transport statistics but also providing a semi-quantitative picture of the transport statistics (e.g., using probability-density representation), across seasons, regions; and interpret the plume pathways and patterns from various contexts (e.g., dynamical pathways). By combining the transport statistics and the resulting database, are designed to answer the many questions, like which synoptic regions are favor short-, mid-, long-, range transport, where the tropospheric, UTLS, stratospheric persists mostly, how these major transport insights are can be utilized for forecasting, operational and mission planning, climate models, infer probable downstream effects to chemical, micro-physical, and radiative impacts.

2. PyroCb inventory and statistical analysis

A newly published global inventory of pyroCb events (Peterson et al., 2025a) provides all pyroCb information use in this study. This inventory compiles occurrences of pyroCbs globally, examining their frequency and variability from 2013 to 2023. Among the 761 worldwide pyroCb events that injected smoke between altitudes of 8 and 18 km, 55% occurred within 1 km of the tropopause or higher, with 69 events (9%) injecting smoke directly into the stratosphere. The 2023 season experienced a record-breaking total of 169 pyroCb events globally, 142 of which occurred in Canada. For our current study, we focused on 545 pyroCbs over North America (excluding 18 Alaskan pyroCbs), which represent 71.6% of the total worldwide pyroCb events.

Figure 1 illustrates hovmöller-style diagrams and map that depict the interannual variability, seasonality, and regional distribution of the 545 North American pyroCb events. The time axis is collapsed to a single reference year to highlight seasonal frequency. In the top half of Fig. 1, the regional dependency of pyroCb occurrence is depicted, with each vertical bar representing a single pyroCb event, color-coded by latitude relative to the US-Canada border (49°N) to facilitate visualization of pyroCbs in Canada and the USA. The bottom half of Fig. 1 presents the pyroCbs color-coded by their maximum injection altitude relative to the local tropopause. While more pyroCbs occur during the spring in Canada (71 events, or 13% of total occurrences), the fall season coincides with more pyroCb activity in the USA (41 events, or 7.5% of total occurrences). During summer, pyroCb events are widespread across North America, with a total of 433 events (74.4% of total occurrences) affecting both regions; however, Canada experiences a significantly higher number (357) compared to the USA (187) (see Fig. 1 and further details in the Results section).

Figure 1 and Fig. S1 reveal intriguing insights regarding the maximum injection altitude of pyroCbs, particularly in terms of variability with latitude, showcasing distinct patterns between Canadian and USA pyroCbs. Most Canadian pyroCbs exhibit maximum injection altitudes within the upper troposphere and lower stratosphere (UTLS) regions, with mean maximum injection heights closely aligned with the mean tropopause height, predominantly just below the tropopause. In contrast, the USA pyroCbs generally exhibit a greater average maximum injection altitude, with the difference increasing to the south. Overall, while the mean injection altitude of USA pyroCbs is slightly higher than that of Canadian pyroCbs, this trend

indicates an increase in mean injection height from the northern Canadian regions to the southern USA. This pattern may be influenced by various factors, including the lower tropopause heights at higher latitudes in Canada, which likely act as a
130 barrier to pyroCb development, limiting vertical penetration into higher altitudes. Despite the overall higher mean injected altitude of USA pyroCbs, a significant portion remains well below the tropopause.

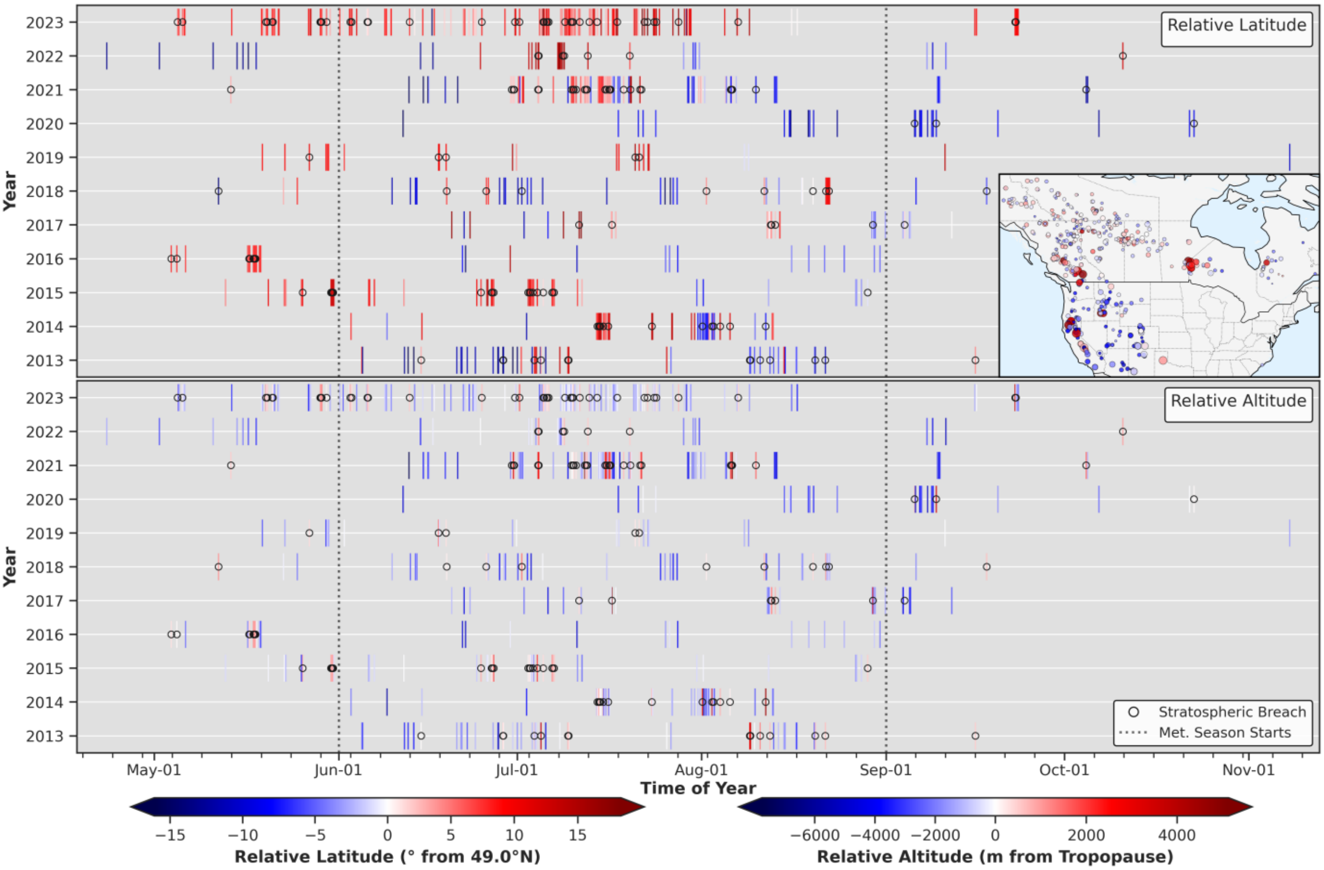

Figure 1. Hovmöller-style diagrams illustrating the interannual variability, seasonality, and regional distribution of 545 North American pyroCb events. The time axis is collapsed to a single reference year to highlight seasonal frequency. (Top panel) Each
135 **vertical bar represents a single pyroCb event, colored by its latitude relative to the US-Canada border (49°N). (Bottom panel) Events are colored by their maximum injection altitude relative to the local tropopause. Vertical dotted lines denote the start of meteorological seasons (MAM for spring, JJA for summer, SON for fall). Across all panels, open black circles indicate stratospheric breaches (events where injection altitude met or exceeded the tropopause). The inset map displays the spatial distribution of these occurrences, colored by relative injection altitude to match the lower panel.**

140 3. Langley Trajectory Model (LaTM)

The NASA Langley Trajectory Model (LaTM) is a kinematic, wind-driven Lagrangian framework that computes 3-D forward and backward trajectories of air parcels from specified latitude, longitude, altitude, and time using gridded meteorological analyses as dynamical forcing. LaTM has supported boundary-layer through stratospheric transport studies since the early 1990s, including foundational work on filamentation and chaotic advection near the polar vortex edge (Pierce and Fairlie, 1993). LaTM integrates parcel positions with a fourth-order Runge–Kutta scheme and interpolates 3-D winds and thermodynamic fields to each parcel location. Along with latitude, longitude, altitude, and parcel age, we also analyzed additional LaTM-derived dynamical variables—particularly potential temperature (θ) and potential vorticity (PV)—to diagnose smoke-plume transport pathways and layer transitions.

Over the past decades, LaTM has been applied across a wide range of transport problems and evaluated through comparisons with independent observations and field-campaign measurements (Vernier et al., 2018; Vernier et al., 2022; Pandit et al., 2024). Beyond stratospheric dynamics and mixing-barrier studies, it has been used to interpret UTLS tracer structure observed during aircraft campaigns, and in air-quality/source–receptor contexts via "Lagrangian sampling" to attribute regional transport contributions to surface pollution and to support accountability/forecast applications. A distinctive capability of LaTM is its integration with spaceborne remote sensing to reconstruct 3-D plume evolution via "trajectory mapping," which has been demonstrated for volcanic aerosol/ash applications and evaluated against CALIOP (Cloud-Aerosol Lidar with Orthogonal Polarization) observations (e.g., Vernier et al., 2013), including UTLS volcanic plume dispersion and interactions with large-scale circulation such as the Asian summer monsoon (e.g., Fairlie et al., 2014).

LaTM has also been applied to biomass-burning problems, including smoke-layer interpretation and plume injection-height characterization using CALIOP and MODIS (e.g., Soja et al., 2012), and more broadly to connect fire-impacted air masses with downwind tracer anomalies. We have similarly used LaTM for pyroCb transport studies (Choi et al., 2020), including event-focused forecasting and mission-planning support. Together, these precedents motivate our use of LaTM here as the central dynamical tool for diagnosing probabilistic pyroCb smoke transport pathways across the troposphere–UTLS–stratosphere, while evaluating smoke presence and tracer behaviour using independent satellite observations (CALIOP, OMPS UVAI, and MLS, brief descriptions of these datasets are provided below).

CALIOP onboard the CALIPSO (Cloud-Aerosol Lidar and Infrared Pathfinder Satellite Observations) satellite is a spaceborne lidar that provides along-track vertical curtain profiles of aerosol/cloud structure, including attenuated backscatter and depolarization information. We used CALIOP Level-1B Standard profiles (CAL_LID_L1-Standard-V4-51, Winker et al., 2009) to document plume altitude and vertical layering for selected overpasses within the event window.

Suomi-NPP OMPS Nadir Mapper (OMPS-NM) is a nadir-viewing UV spectrometer; its UV Aerosol Index (UVAI) is a standard diagnostic for UV-absorbing aerosols such as smoke. We processed the OMPS L2 NM Aerosol Index product (NMMIEAI-L2, V2; Torres, 2019) over the event day and following 7 days to evaluate aerosol presence and horizontal dispersion in a manner consistent with our transport diagnostics.

Aura MLS (Microwave Limb Sounder) is a limb-sounding microwave radiometer that provides vertically resolved trace-gas information and gridded Level-3 fields. We used the MLS Level-3 Daily Binned Carbon Monoxide product (ML3DBCO, V005; Schwartz, 2021) for each pyroCb event day and the subsequent 7 days, using the same regional/time-window sampling applied throughout the study.

To initialize LaTM, we used the pyroCb source latitude/longitude, event time, and estimated maximum injection altitude from our North American PyroCb database (545 events, 2013–2023). For each event, trajectories were released as a single vertical column at the source location and initialized from the maximum injection altitude down to 5 km below it, using 100 m vertical spacing (i.e., $z \in [z_{\mathrm{max}}\boxed{f_0}-5$ km, $z_{\mathrm{max}}\boxed{f_0}]$ in 0.1 km increments). Thus, the absolute altitude range varies by event and is not fixed in ASL; the 5 km depth is defined relative to each event's $z_{\mathrm{max}}\boxed{f_0}$. Beginning trajectories within a 5 km vertical layer allows for the deep "chimney" configuration of a pyroCb injection, ensuring that the model accurately represents the entire mass of the smoke plume as it disperses under different wind speeds and directions at various altitudes. Future work may further refine the trajectory-release configuration for targeted sensitivity analyses. To represent sustained injection in a consistent manner across events, releases were distributed over a 2 h window starting at the event time. Forward trajectories were integrated for 7 days, and trajectory output (e.g., latitude, longitude, altitude, age, PV, and θ) was saved at hourly intervals.

Meteorological context and trajectory modelling relied on data from NASA's MERRA-2 (Gelaro et al., 2017), which supply three-dimensional fields of wind, temperature, and dynamic atmospheric variables necessary for simulating plume transport and investigating sensitivity to meteorological conditions. Original latitude and longitude resolutions are 0.5° to 0.625°; data was coarsened by a factor of 2, and native 3-hourly data was interpolated to 15-minute increments to run the trajectory model.

Tropopause height was taken from the Reanalysis Tropopause Data Repository, using the ERA5-derived 1° × 1°, 6-hourly product, (Hoffmann and Spang, 2022) and used to compute tropopause-relative parcel altitude and to define the troposphere/UTLS/stratosphere layers.

Trajectory positions were mapped to a regular latitude–longitude grid at 1° × 1° resolution using all hourly parcel locations (i.e., each grid cell is incremented each time a parcel occupies it). For each grid cell, we computed a normalized occurrence probability ("trajectory PDF") as the ratio of number of parcel–time samples falling within the cell to the total number of parcel–time samples over the selected event set and time window. If multiple parcels (or the same parcel at different hours) pass through a grid cell, all samples contribute to the count. Vertical cross-sections (latitude–altitude and longitude–altitude) were computed using the same approach, with altitude binned at 250 m resolution. These PDFs represent the relative likelihood of parcel presence (and therefore plume occurrence) within each bin. For age, altitude, θ, PV, and tropopause-related quantities, we also computed grid-cell summary statistics (mean, median, and selected percentiles) from the samples contributing to each grid cell/bin.

For MLS and OMPS, we built an event-centred date list consisting of each pyroCb event date and the subsequent 7 days. We then combined all unique dates across all events and extracted the satellite fields for those dates to compute the gridded statistics. Aura MLS Level-3 daily binned CO fields were sampled on the MLS daily grid and summarized by grid cell across all event-centred days using consistent statistics (median, mean, and selected percentiles). OMPS UVAI swath pixels (daytime only) were binned to the same analysis grid and summarized in the same way. Here, "percentile" refers to the percentile of all values contributing to a given grid cell across the full event-centred sample (days 0–7 over all events). This enables direct comparison between satellite-derived tracer/aerosol signatures and the trajectory-based transport diagnostics. Further details on LaTM configuration, trajectory post-processing choices, and instrument-specific filtering/quality control for the MLS, OMPS, and CALIOP datasets are provided in the relevant sections. The combination of these tools and datasets provided a comprehensive framework for analysing the occurrence, transport, and atmospheric effects of pyroCb events.

4 Trajectory Model Demonstration and Validation

The Chuckegg Creek Fire has been chosen for this case study and validation process for several compelling reasons. One of the primary factors in selecting this specific event was the occurrence of multiple CALIPSO overpasses during the initial days following the pyro-convective cloud (pyroCb) transport. This abundance of data enhances the robustness of our validation efforts. The Chuckegg Creek Fire pyroCb occurred in Alberta, Canada, near coordinates 58.1°N and 117.1°W, on June 17th, 2019, at 20:00 UTC (Peterson et al., 2025a). The first pulse lasted about five hours, ending around 01:00 UTC on June 18th, followed by another pulse near 02:00 UTC that lasted about an hour. According to the Fort Smith sounding, the injected altitude was around 12.7 km. For additional context, there was another pyroCb at the same location on June 18th at 23:00 UTC that reached about 10 km, and another smaller pyroCb at a nearby location (59.7°N and 116.9°W) on June 17th at 20:20 UTC that reached approximately 10.7 km. Since this is a case study and validation of the LaTM, we decided to use the more appropriate sustained duration of seven hours (from 20:00 UTC to 03:00 UTC the next day) for the pyroCb. This was done to treat the continuous injection collectively rather than analysing the pulses separately. We initialized the air parcels from 13.7 km (12.7 km plus 1 km to account for uncertainties) down to 8.7 km, resulting in an average smoke layer thickness of 5 km, which is similar to the climatological smoke thickness used for all the pyroCb trajectory runs in our current study. Since this specific event was larger than the climatological mean, we opted to initialize the air parcels over a 100 km radius instead of using a single-column approach. The vertical grid size was 100 m and the timestep was 15 minutes for the case study and the decadal LaTM runs.

We compared the LaTM results (altitude vs. latitude PDF contour, Fig. 2 (top)) with the total attenuated backscatter and depolarization ratio from CALIPSO/CALIOP. First, the air parcels from LaTM were filtered within +/- 1 hour of the CALIPSO orbit track timestamp. Then, the filtered air parcels were further sorted based on their proximity to the CALIPSO orbit track, within 100 km, to prevent aggregation over a large longitudinal distance within the +/- 1 hour timeframe. The PDF was calculated on a 1-degree latitude and a 0.5 km altitude grid. We compared the LaTM results against CALIPSO data for the first seven days. On day one (2019-06-18 at 10 UTC), the CALIPSO data showed a smoky layer centred at an altitude of 12.5 km and a latitude of 62 degrees. Although the backscatter and depolarization ratio values were higher than typical for smoke layers, their alignment in both altitude and latitude suggested that it could be a smoky-ice layer resulting from the Chuckegg Creek pyroCb event (Fromm et al., 2021). Above approximately 64 degrees latitude, the presence of the smoke layer became more evident, indicated by the usual backscatter and depolarization values associated with smoke layers (Kim et al., 2018, Peterson et al., 2018, Fromm et al., 2008). On day two (2019-06-19 at 09 UTC), the LaTM clearly models the smoke layer, showing a near identical latitude span and altitude alignment compared to the CALIPSO total attenuated backscatter and depolarization values, which reflect typical smoke layer characteristics. On day three (2019-06-20, 20 UTC), the CALIPSO data, which was sampled during the daytime (unlike the other six days when the data was collected at night), appeared noisier but still indicated a smoke layer between 62 to 65 degrees latitude. The LaTM effectively captured the overall plume layer. On day four (2019-06-21 at 09 UTC), the CALIPSO data reveals two distinct smoke layers at similar altitudes. The layers appear separate because they were sampled as they spiralled. The LaTM effectively captures the two separate layers. On day five (2019-06-22 at 08 UTC), the CALIPSO data shows a continuous smoke layer stretching from approximately 44 to 60 degrees latitude. The LaTM accurately modelled the smoke layer that aligns perfectly with this observation, demonstrating a matching distribution in both latitude and altitude. On day six (June 23, 2019, at 07 UTC), the CALIPSO data reveal two distinct layers. The layer with the highest concentration is centred around 40 degrees latitude and has a tapered, inclined shape. Additionally, another layer of high concentration can be observed around 60 degrees latitude. Both layers have been modelled relatively well with LaTM, particularly when examining the locations of the highest PDF values. On day seven (June 24, 2019, at 06 UTC), the CALIPSO data indicate a vertically inclined layer centered at 50 degrees latitude, along with another concentrated layer at 55 degrees latitude and 12 km altitude. The LaTM plots match closely with these locations in terms of both latitude and altitude, especially when considering the areas with the highest PDF values.

We also compared the LaTM-modeled transport of the pyroCb smoke layer against the OMPS Aerosol Index (AI) observations using a geospatial latitude and longitude map (in the left and right columns, Fig. 2 (bottom)). The LaTM-modelled air parcels were filtered to fall within +/- 2 hours of the OMPS orbital track timestamp, represented by a solid line in Fig. 2 (bottom). The adjacent two orbital tracks are also shown to illustrate the relative position of the smoke more clearly on the map. The PDF contour map from LaTM was calculated on a 0.25-degree latitude and longitude grid. We examined the smoke transport modelled by LaTM against OMPS AI for the first seven days, finding a strong agreement between the modelled transport and the observations. On day one (2019-06-18, 18:42 UTC), the modelled smoke PDF map indicated that LaTM effectively captured the transport of smoke. The OMPS-AI observations displayed a similar spatial distribution and shape of the smoke layer, with the highest AI values located in the same areas as the highest PDF values. On day two (2019-06-19, 18:23 UTC), the OMPS AI revealed that most of the smoke was positioned west of the centre orbit, as accurately modelled by LaTM. Only an edge or tail of the smoke appeared on the east side of the centre orbit, a detail that LaTM also captured. This indicated that the overall shape and distribution of the LaTM-modelled smoke transport were in good agreement with the observations. On day three (2019-06-20, 18:04 UTC), OMPS AI observations confirmed that LaTM had effectively modelled the smoke transport, evident in the accurate representation of the b-oomerang-like shape and distribution of the smoke. The highest OMPS AI values again correlated closely with the highest PDF values on the contour map. On day four (2019-06-21, 17:45 UTC), OMPS AI observations illustrated a V-shaped plume near Hudson Bay, which was similarly modelled by LaTM. The relative positions of the plume were in good agreement with OMPS-AI observations.

https://doi.org/10.5194/egusphere-2026-3536
Preprint. Discussion started: 6 July 2026

From day five (2019-06-22, 17:26 UTC) onward, the plume began to stretch and spiral away. The lower-level smoke transport was slightly slower and shifted southward, while the higher-level smoke layer moved more quickly eastward, remaining further north. On this day, the OMPS AI indicated a smoke layer signature within a box of approximate latitudes 40°N to 60°N and longitudes 56°W to 78°W, with a boomerang-like filamentary shape. LaTM effectively modelled this shape and distribution, especially for the higher-level smoke layer observed within similar geographic bounds. By day five, the lower-level smoke layers began to detach from the higher-level smoke west of approximately 78°W. These layers continued moving slowly southward, a trend visible in the maps for days six and seven. It is noteworthy that the lower levels of smoke were not detected by the OMPS AI. The OMPS Aerosol Index (AI) exhibits significant altitude sensitivity, being much more responsive to high-altitude smoke than to plumes in the mid to low troposphere (Fromm et al., 2008). This sensitivity arises from the absorption of Rayleigh-scattered UV radiation from the atmospheric column beneath the aerosol layer. On day six (2019-06-23, 17:07 UTC), the OMPS AI indicated that the smoke layer had spread from 35N, 65W to over Greenland, and the LaTM accurately represented the shape and distribution of the smoke. As mentioned earlier, the lower-level, slower-moving southern smoke layer was not evident in the OMPS AI signature on days six and seven. On day seven (2019-06-24, 16:48 UTC), the OMPS AI signature appeared weaker but was still visible, particularly in areas of higher smoke concentration. LaTM continued to model the smoke layer effectively, even on the seventh day. On days six and seven, including the OMPS-AI data from the orbital track near Greenland and Iceland, it shows a signature in that region, as illustrated in Fig. S3.

We also conducted a rigorous sensitivity analysis of the model parameters (e.g., the number of initialized air parcels in a single column at the pyroCb plume center location versus distributing the air parcels over a radius around the center, sustained hours, injection heights) (Figs. S3-S4). Overall, the LaTM models the transport of pyroCb smoke within reasonable bounds, especially when examining an ensemble map (as we did in the probabilistic way using PDF). Here, the “ensemble” refers to the set of LaTM trajectory realizations initialized using multiple release points, altitudes, and/or times to represent uncertainty in the smoke injection location and height. The ensemble-based probability density function (PDF) maps summarize the regions most frequently sampled by the trajectory members and therefore provide a probabilistic view of the likely smoke transport pathway. In addition to these ensemble/PDF maps, we examined individual trajectory paths, altitude-dependent trajectory evolution, sensitivity to initialization height and location, and comparisons with satellite-observed smoke features to assess the consistency of the modelled transport. In Fig. S3, a comparison of two runs that involved the Chuckegg Creek pyroCb event is shown. One run involved initializing air parcels over a 100 km radius, while the other run involved a single-column initialization of the air parcels (the approach we used for climatological 545 pyroCb LaTM runs). Both runs qualitatively produced similar transport pathways when compared to CALIPSO backscatter, depolarization, and OMPS AI.

The analysis of the case study and comparisons of the LaTM transport results against CALIPSO and OMPS observations established that LaTM accurately models the transport of pyroCb smoke. Also, visually comparing the results from LaTM against those from the NAME model (Osborne et al. 2022) suggests that LaTM better models the transport of the pyroCb than NAME does. There could be several reasons why LaTM performs better than NAME, but this is outside the scope of this study. This indicates that LaTM can be used for further similar studies of single events or climatological transport of pyroCb smoke.

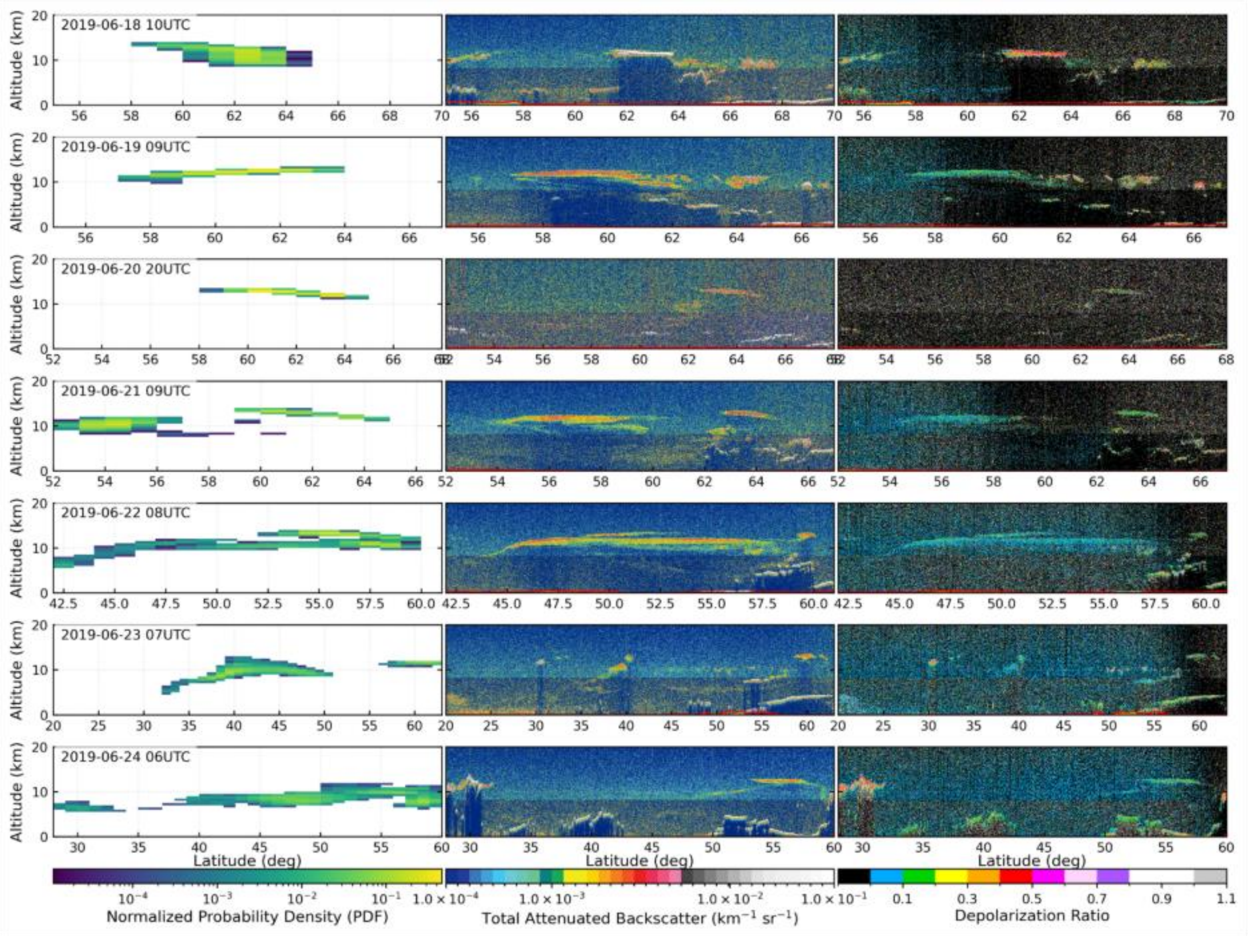

https://doi.org/10.5194/egusphere-2026-3536
Preprint. Discussion started: 6 July 2026

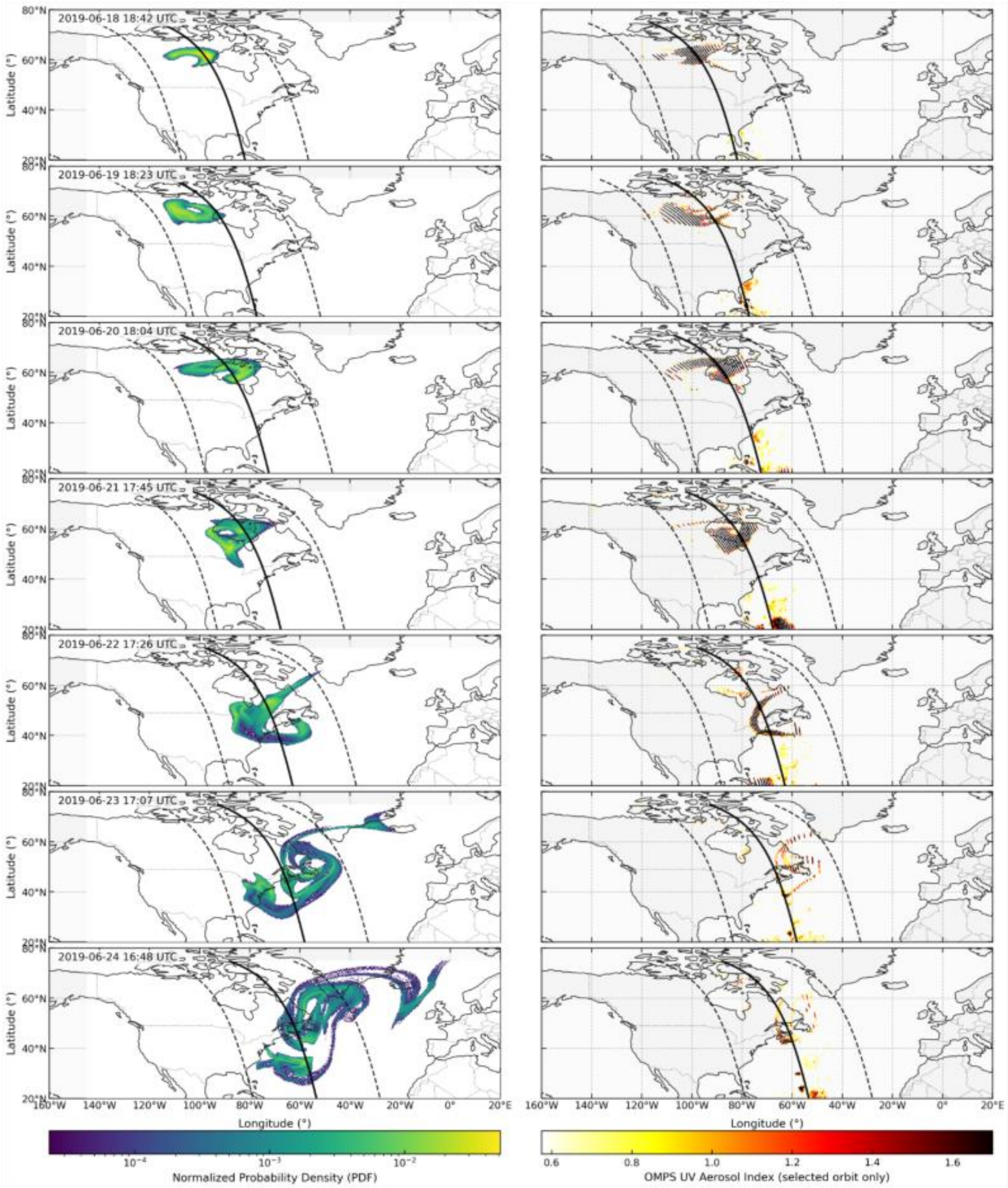

Figure 2. Panels showing daily comparisons of key variables following the Chuckegg Creek (58.1N, 117.1W, 20190617 20 UTC) event. For each day, the panels include: (top, 1st column) vertical cross-sections of trajectory model output extracted along CALIPSO orbit tracks within +/- 100 km, (top, 2nd column) CALIPSO total attenuated backscatter profiles, (top, 3rd column) CALIPSO depolarization ratio profiles, (bottom, left column) latitude–longitude PDF maps of trajectory air parcel positions, and (bottom, right column) OMPS Aerosol Index (AI) distributions. These visualizations collectively illustrate the evolution and spatial distribution of smoke plumes over the first seven days.

https://doi.org/10.5194/egusphere-2026-3536
Preprint. Discussion started: 6 July 2026

5 PyroCb Smoke Transport from North America

5.1 Transport Overview: Spatial Footprints, Altitude Distribution, and Plume Age

We examined the decadal diagnostics of pyroCb plumes transport from several points of view to get as many insights as possible into the pyroCb transport. Figure 3 shows the global transport of the pyroCb smoke as a PDF (top), the average age of the smoke (middle), and the average altitude of the pyroCb air parcels (bottom). The PDF shows the comparative distribution of the air parcels from the North American pyroCbs, mostly several transport hotspots (localized maxima). There is a local maximum in the north-western region of Canada (approximately around 120°W, 57°N, for a closer look, see Fig. S7), primarily representing the fresh (less than one day) smoke around the area. And there is another local maximum surrounding the west-central region of USA (approximately around 102°W, 38°N), with relatively fresh smoke layers (less than one day, for a closer look, see Fig. S7). There is another local maximum (90°W, 35°N) away from the pyroCb locations representing mostly the downstream mid-range older (around 1-2 days) smoke. We also ranked the highest probability locations (please see Fig. S7 in supplementary materials, for better understanding and visualization).

The PDF clearly shows a main transport pathway for the long-range air parcels that heads towards Europe around a longitudinal line of 45°N. The smoke layers approximately take 4-5 days to reach Europe. The average height of the smoke layers that head over to Europe around 10 to 11 km, mostly representing the UTLS layers. These contour maps also reveal some interesting insights about the transport of smoke layers into the tropics. Although the trajectory density of transport into the tropics is low, the mean-altitude contours indicate that the parcels reaching tropical latitudes reside high in the upper troposphere/ Tropical Tropopause Layer (TTL): a subset lies above ~15 km, near/above the TTL base defined by the level of zero net radiative heating (≈14.5–15 km). Air detraining above this level experiences net radiative heating and tends to ascend, so these parcels could continue rising and potentially reach the lower stratosphere on longer timescales (Fu et al., 2007).

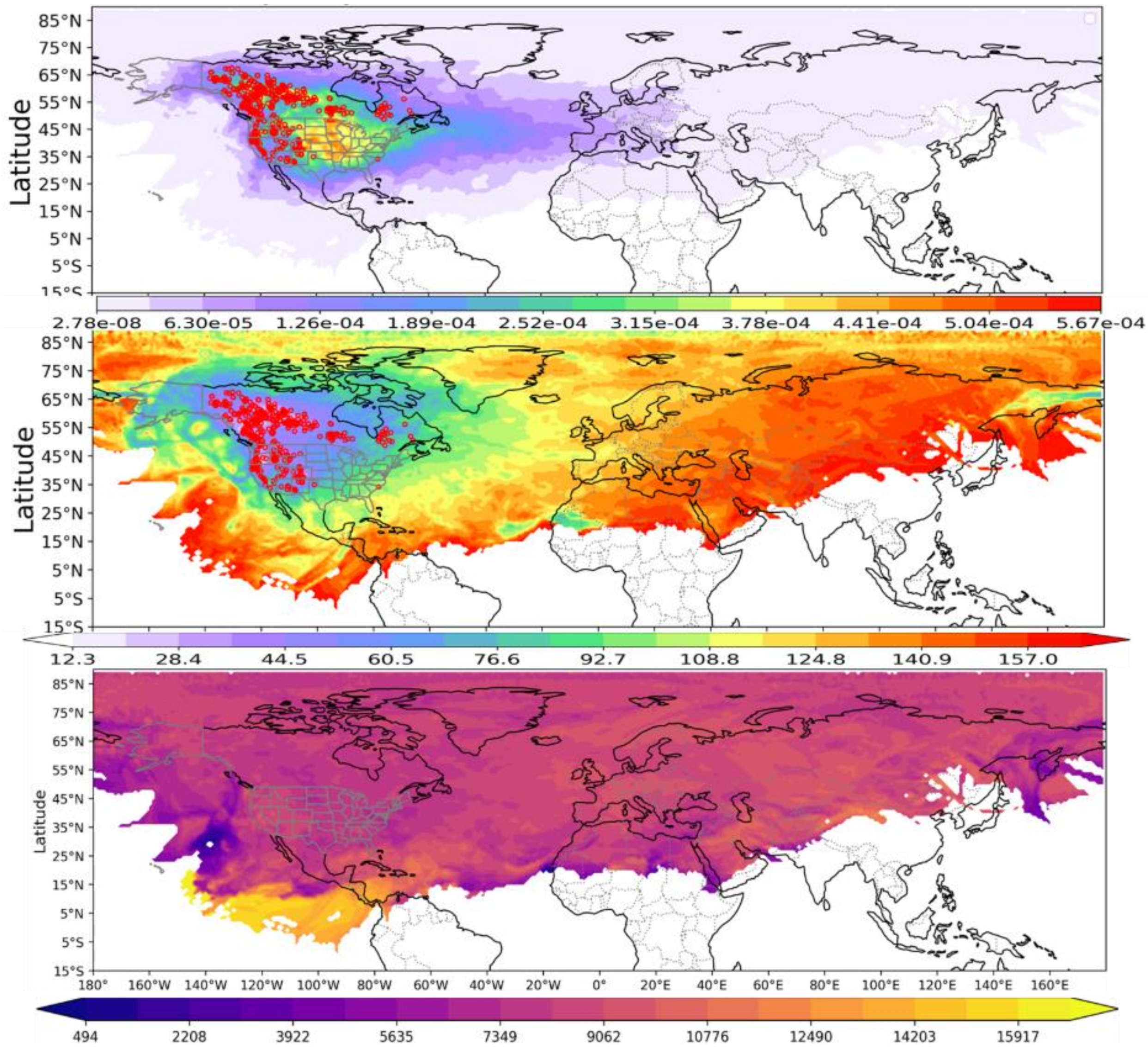

Figure 3. Top: probability density function (PDF) of smoke air-parcel concentrations, with color bar showing normalized trajectory density [unitless]. Middle: plume mean age since injection, with color bar showing age since injection [hours]. Bottom: plume mean altitude, with color bar showing altitude [m]. These panels collectively illustrate the statistical spatial properties, temporal evolution, and vertical distribution of pyroCb-derived smoke plumes.

5.2 Seasonal and Regional Dependence of Transport Pathways

Figure 4 shows the seasonality and regionality of the pyroCb occurrences and their associated plume transport. To better reveal long-range transport pathways—where trajectory densities are low because of the 7-day integration window—please see the PowerNorm-scaled (PDF$^{\gamma}$) version in Fig. S9. There is a clear pattern in seasonality, in both pyroCb occurrence and downstream transport, since seasonal changes in event frequency/location and in large-scale circulation jointly control the transport pathways. Most of the spring pyroCb (71 or 13% of total events) activity takes place over Canada resulting in the main transport pathway being further north compared with other seasons, frequently affected by the polar or mid-latitude jet streams. Most of the fall pyroCb (41 or 7.5% of total events) takes place in the USA; the transport pathways follow westerly winds, and southern smoke layers are caught in the sub-tropical jet.

One interesting feature in the pdf of the fall transport is the presence of an accumulation zone around 20°N to 30°N and 120°W to 130°W. This accumulation is notable because it lies southwest of the pyroCb sources, contrary to the typically eastward flow. Another accumulation zone in the fall pdf is near Hudson Bay (~55° N, 85° W), suggesting increased residence rather than simple downstream through-transport. A few fall pyroCb over Canada follow the transport pathways more north-eastern bound. The summer season (433 or 74.4% of total events) affects both regions, although Canadian regions have a higher frequency of pyroCbs. Canada has almost double the number of pyroCbs compared to the USA, with 357 recorded against 187 from 2013 to 2023 across all seasons. The transport pathways from the Canadian pyroCbs moves to the south as they travel further east, eventually following the 40th North parallel for the long-range transport towards Europe. Although the transport pathways of the USA pyroCb plumes follow a track heading to 30N for the short- to mid-range transport, the mid- to long-range transport gets eventually diverted further north (around 40N) while heading towards Europe.

https://doi.org/10.5194/egusphere-2026-3536
Preprint. Discussion started: 6 July 2026

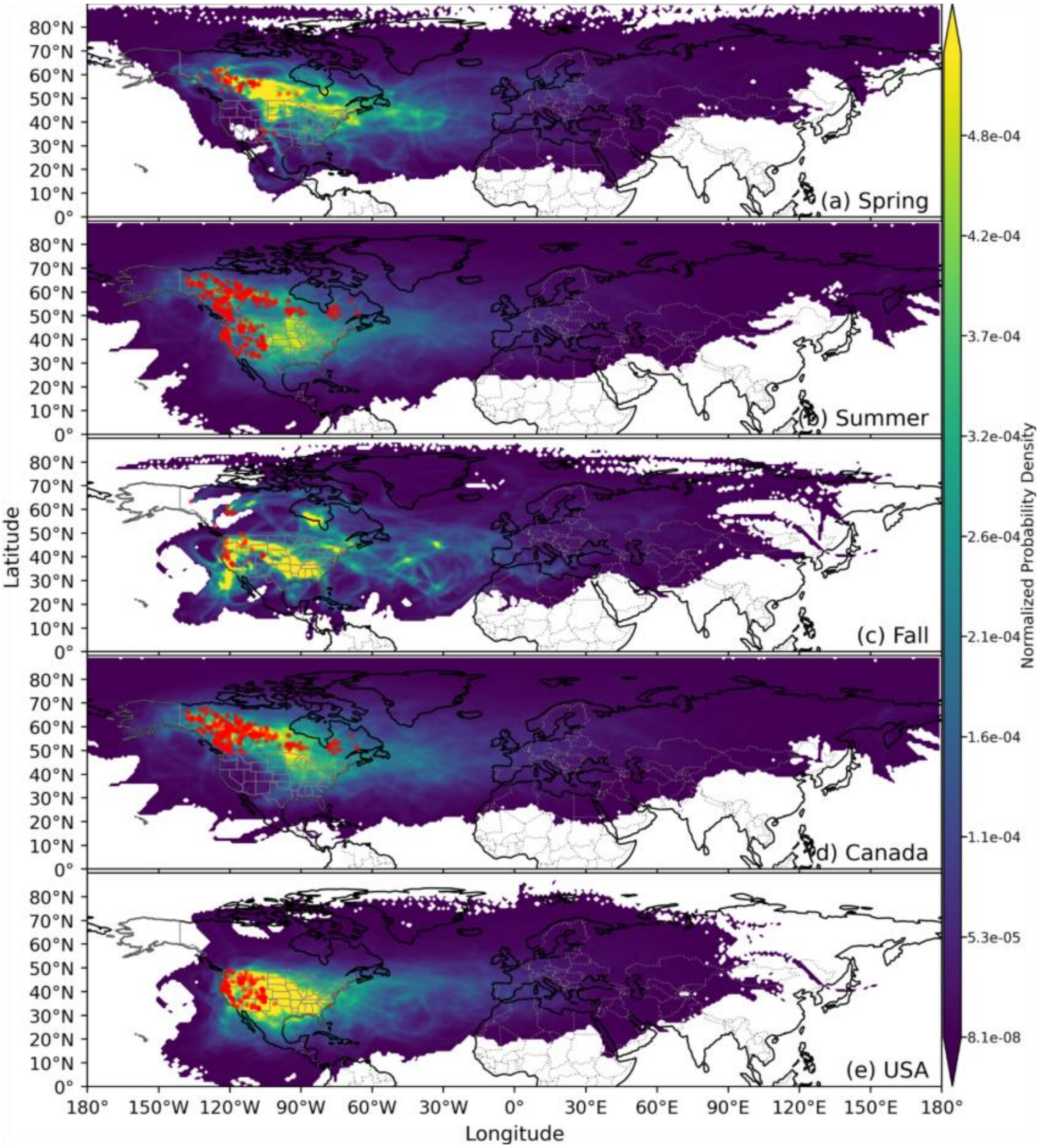

Figure 4. Seasonality and regionality of pyroCb smoke transport. The subplots a, b, and c show the seasonal distribution of smoke transport, categorized into spring, summer, and fall. The subplots d and e illustrate the regional differences in smoke transport, divided between Canadian and USA pyroCb events. The red dots are pyroCb locations.

5.3 Transport in Distinct Vertical Regimes: Troposphere, UTLS, and Stratosphere

Figure 5(top) shows the transport of smoke injected above the tropopause. The stratospheric smoke plumes are more frequent around a latitude band between 35°N and 65°N with the highest frequency around 50N while transported toward

Europe. The maximum concentration of the stratospheric smoke layer near 50° N appears to be primarily associated with transport from three major pyroCb source hotspots where many of the strongest events injected smoke to higher altitudes: southern Oregon/northern California near the Cascade Range (~42° N, 122° W), interior British Columbia near the Cariboo–Thompson/Wells Gray region (~52° N, 120° W), and northern Manitoba near the Hudson Bay–Lake Winnipeg sector (~53° N, 95° W). As shown in Figs. 1 and 5, smoke originating from the southern Oregon/northern California hotspot is first transported north-eastward before merging with the broader midlatitude transport corridor near 50° N. This pathway helps explain why the stratospheric transport maximum is centered near 50° N, rather than directly over the source regions. The result suggests that the observed stratospheric concentration maximum reflects both the locations of high-altitude pyroCb injections and subsequent synoptic-scale steering by the midlatitude circulation. Fewer stratospheric plumes travel to the Equator.

The transport pathways of the UTLS layer (Fig. 5 (middle)) are dominated by the Canadian pyroCbs as expected since their maximum injection heights is usually near the tropopause, located at lower altitudes at higher latitudes (Figs. 1 and S1). The UTLS transport pathway is centered around a latitude band between 30N and 75N, although the layer gets thinner and narrower as the smoke travels east by the westerlies, centered around 45N. The tropospheric smoke (Fig. 5 (bottom)) frequency is higher further south for the short- to mid-range transport, with a higher frequency up to 30°N, eventually, although the tropospheric layer shifts north when traveling mid- to long-range around the same centerline as the UTLS layer, around 45°N. Only a few UTLS and tropospheric smoke layers show cross-hemispheric transport into the southern hemisphere. Absorbing aerosols in the stratospheric layers (black and brown carbon) can experience enhanced solar heating, leading to diabatic ascent (“self-lofting”) by several kilometers (Das et al., 2021; Yu et al., 2019). In some cases, stratospheric smoke also organizes into long-lived smoke-charged anticyclonic vortices (often termed SWIRLs), which can further prolong residence time by dynamically confining the plume in the stratosphere. LaTM does not simulate SWIRL dynamics, though MERRA-2 may partially capture their large-scale circulation signatures.

This section summarizes 7-day transport across the troposphere, UTLS, and stratosphere for parcels initialized within the PyroCb injection envelope (2013–2023). Because the trajectories are passive and conditioned on PyroCb event timing, location, and injection-height range, the results characterize PyroCb-conditioned transport pathways and are not a climatology of background (non-PyroCb) parcel transport.

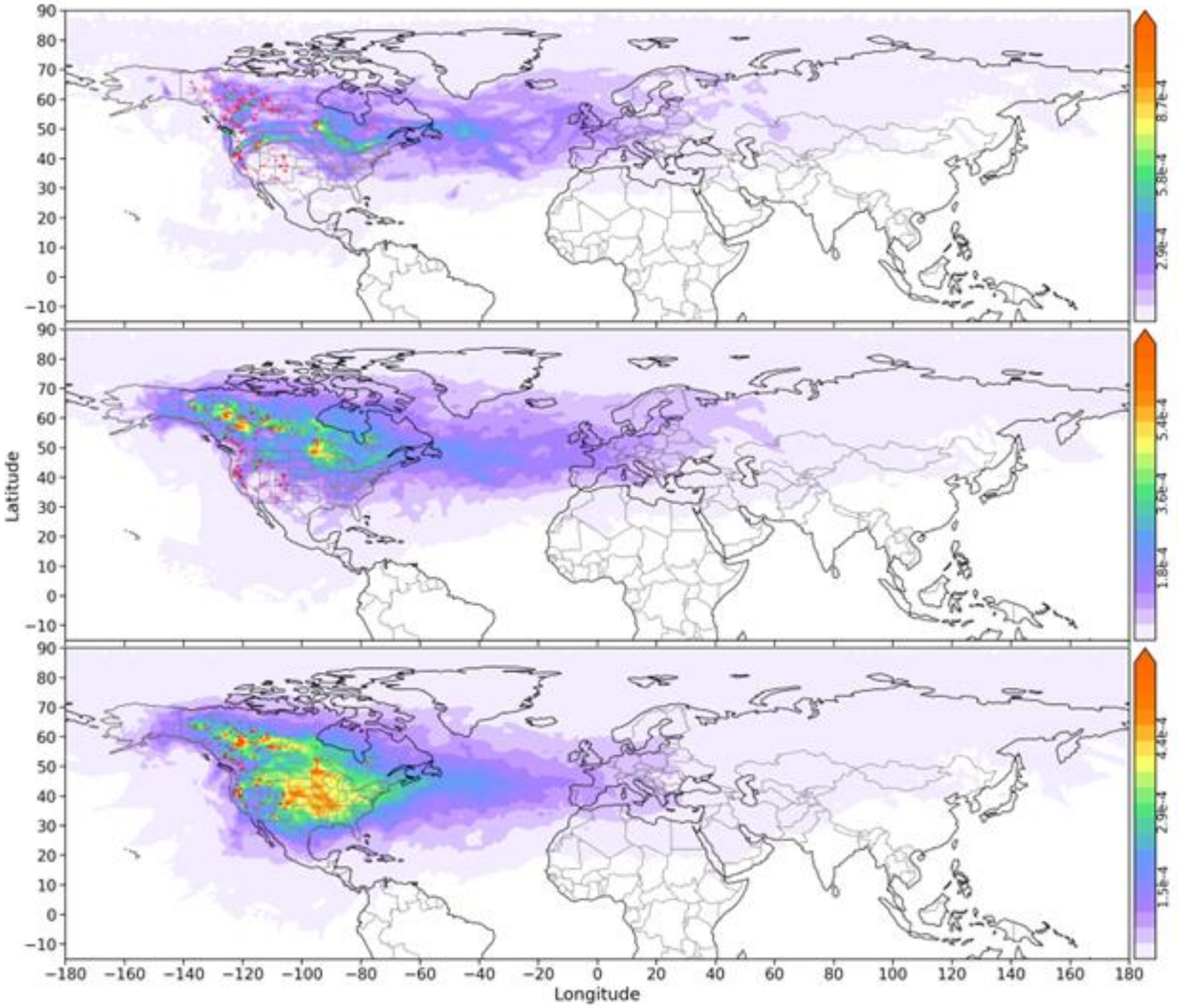

Figure 5. Maps illustrating the transport pathways of pyroCb smoke plumes in different atmospheric layers: stratospheric (top), the upper troposphere–lower stratosphere (middle) (UTLS; defined as +2 km and −2 km relative to the tropopause), and tropospheric (bottom). These maps highlight the distinct spatial distribution of smoke transport within each layer. The colorbars show normalized probability density functions (PDFs; unitless).

5.4 Vertical Structure and Evolution of Smoke Layers

Figure 6 shows the vertical structure, spatial distribution, and residence time of the pyroCb smoke with absolute altitude and regridded relative-to-tropopause altitude. In the longitude vs altitude plots (Fig. 6a and b), data are latitudinally aggregated and in the latitude vs altitude plots (Fig. 6c and d), data are zonally aggregated. The tropopause-relative altitude diagnostics show that some pyroCb smoke layers extend 6–7 km above the tropopause, confirming that a subset of events injects smoke well into the stratosphere. The PDF values decrease with increasing height above the tropopause, indicating that these highest-altitude layers are relatively less frequent and are associated with the most extreme injection events. Consistent with the stratospheric transport patterns discussed in the previous section, the strongest signal occurs near the 50° N latitude band, beginning near 120° W and extending downstream along the long-range transport pathway. The latitude vs altitude plots (Fig. 6c and d) show two centers (one at around 45N and one at around 60N) of higher concentration in the upper atmosphere close to the UTLS. The two centers are separated by a lower concentration of smoke layer around 50N, possibly due to the mid-latitude jet (also changes in the location of the jet, further north in summer) that accelerates and separates the smoke layer from the further southern part. Another possible reason could also be the locations of Canada and US pyroCbs, see Figs. 1 and S1. Below 60N, the tropospheric smoke appears at lower levels as it moves to the south, almost following isentropic lines (Fig. 6c, also see supplementary Fig. S5).

In the tropics (20N to 10S), smoke layers appear to ascend through the tropical UTLS (Fig. 6c and d; Fig. S5). In tropical regions, large-scale slow ascent through the tropical tropopause layer (TTL) and tropical upwelling into the lower stratosphere—part of the upwelling branch of the Brewer-Dobson circulation—offers another route for tracers that reach the TTL, a pathway that would be better assessed with longer trajectory integrations than the 7-day window used here. Above 60N the tropospheric smoke travels to the north, without any major descending, rather sometimes with ascending, especially the upper-level smoke. Some tropospheric smoke can be transported into the UTLS through several pathways. One of these pathways is direct convective injection, which can occur during events like deep convection that overshoot into the UTLS, although efficacy of this transport mechanism is hard to quantify (Fromm et al., 2019). Additionally, smoke layers that absorb heat can experience diabatic radiative heating, a process known as "self-lofting." This mechanism causes sustained upward movement, lifting smoke from the free troposphere toward the tropopause and even deeper into the lower stratosphere. Although currently the LaTM does not model this process, the temperature profiles assimilated into MERRA-2 may include some thermal effects of large pyroCb plumes.

In extratropical regions, synoptic-scale cyclones and warm conveyor belts (WCBs) can lift smoke air into the UTLS (Khaykin et al., 2025), which may be followed by stratosphere-troposphere exchange (STE) (see supplementary Fig. S6 for more details). Near the jet stream and the dynamical tropopause, phenomena such as tropopause folds, upper-level fronts, and Rossby-wave breaking lead to filamentary intrusions and strong potential vorticity (PV) gradient distortions. This promotes STE by mixing tropospheric and stratospheric air masses. Turbulence, including gravity-wave-induced turbulence, can enhance this mixing and render the exchange irreversible, although such sub-grid scale processes are not explicitly resolved in the current trajectory analysis.

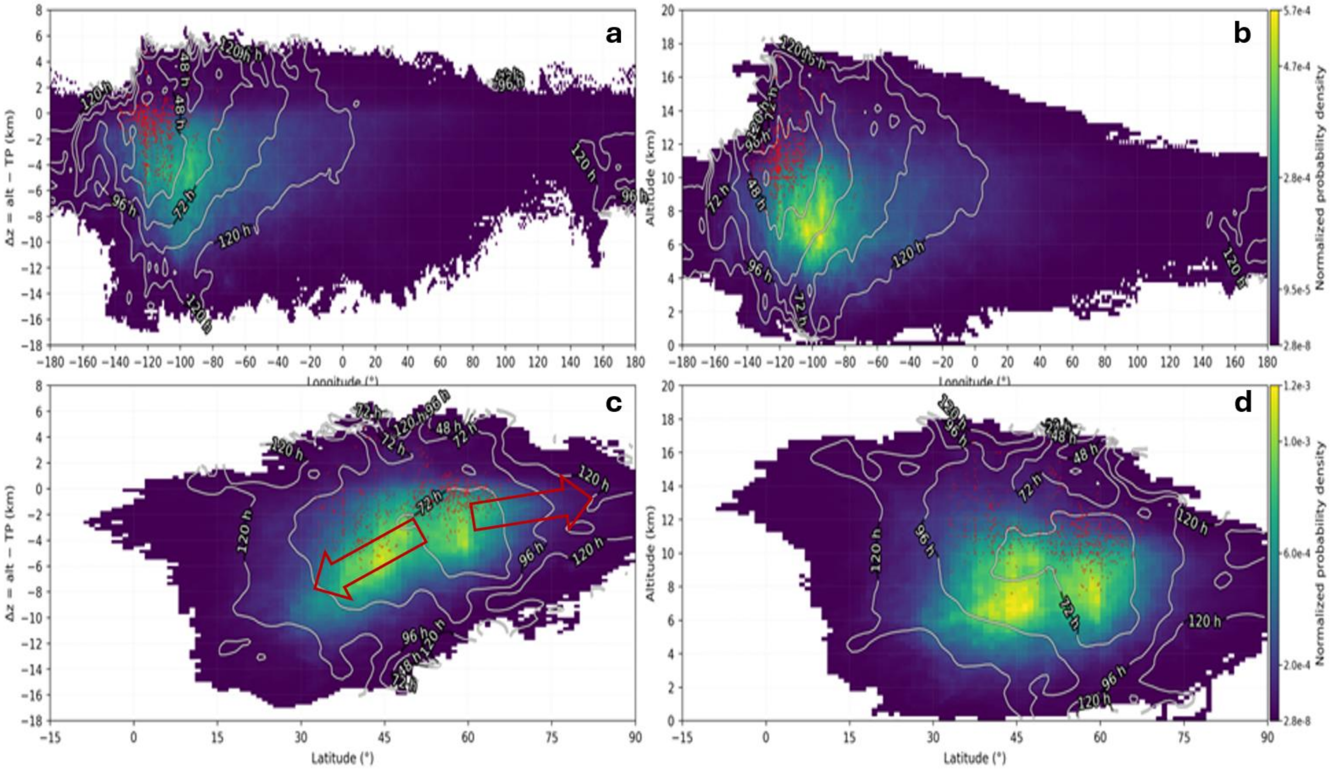

Figure 6. Vertical structure, spatial distribution, and residence time of pyroCb smoke transport. Panels show (a) longitude versus tropopause-relative altitude, (b) longitude versus absolute altitude, (c) latitude versus tropopause-relative altitude, and (d) latitude versus absolute altitude. The longitude–altitude panels (a, b) are aggregated over latitude, while the latitude–altitude panels (c, d) are aggregated over longitude. Color shading represents normalized probability density (unitless), indicating where transported smoke is most frequently located in the projected longitude–altitude and latitude–altitude distributions. Contour lines show the mean smoke age/residence time. Red arrows indicate the dominant projected transport direction, consistent with the transport-vector patterns shown in Fig. S5.

6 Multi-Sensor Corroboration of Transport Pathways

Figure 7 shows the comparison of the pyroCb transport pathways (Fig. 7c) with the OMPS 99th percentile (smaller percentile variations do not affect the contour significantly) AI (Fig. 7a) and MLS 99% percentile CO mixing ratio (Fig. 7b). The pyroCb transport pathways match relatively well with both of them. However, OMPS AI maximum is located further north compared to the maximum frequency of pyroCb plumes. In addition, MLS CO maximum concentration is a little south of the pyroCb transport pathways, although the highest hotspot of the MLS-CO concentration matches quite well with the hotspot of the pyroCb transport pdf. The major differences among the three contour maps are within early hours of fresh smoke transport within short-range transport. As the smoke travels further to the east under the influence of westerlies mid-range to long-range as they approach Europe, their concentrations have a centerline around 50N, proving that main transport corridor is the same for those pyroCb smoke aerosols and their associated trace gases (e.g., CO).

The likely reason for the apparent difference between the LaTM pdf output and the OMPI-AI is that the latter is more sensitive to high-altitude smoke layers. Because the tropopause is generally lower at higher latitudes, Canadian pyroCb injections can more readily place absorbing smoke near or above the tropopause (in the UTLS/lower stratosphere); all else equal, a higher aerosol layer height increases the UV aerosol index, so elevated Canadian layers are expected to exhibit higher AI. In addition, we have seen this in the validation section of the case study. Since the higher-altitude smokes are more sensitive to UV radiation, even at diluted concentrations after a few days, that's why we see better match of the OMPS-AI with LaTM pdf map for the mid- to long-range plume around the 50N centerline as the smoke travels over Atlantic approaching to Europe. The relative higher concentration of OMPI-AI above 70N is mainly due to the influence of the Siberian pyroCb as evidenced in the tail of the signature gets extended when they approach North America, shifting a little bit towards the pole.

The main reason for the apparent difference between LaTM map and MLS-CO is that the tropical and subtropical influence of fires on the signature of CO trace gas from the North American pyroCbs, especially the influence of Asian (ASMA) CO extended to North America as evident by the tail that is moving to North America while shifting further north. Here we compared the MLS-CO at single pressure levels of 215 hPa (approximately 11.3 km), varying the altitude range does not change the heatmap significantly, but including more tropospheric data shifts the pattern further south, as it intuitively makes sense due to higher influences of the CO in the tropics and subtropics. Future work could apply multivariate decomposition methods (e.g., PCA/SVD) to separate dominant modes of variability and evaluate potential confounding influences (e.g., monsoon-related circulation), but such analyses are beyond the scope of this study. Future comparisons of AI and CO with the LaTM could be significantly improved by using the trajectory data to explicitly track the evolving plume. Additionally, incorporating MLS ozone (O_3) would provide a robust chemical filter; by leveraging the natural anticorrelation between O_3 and CO, tropospheric interference can be rigorously screened out to isolate the true UTLS signal.

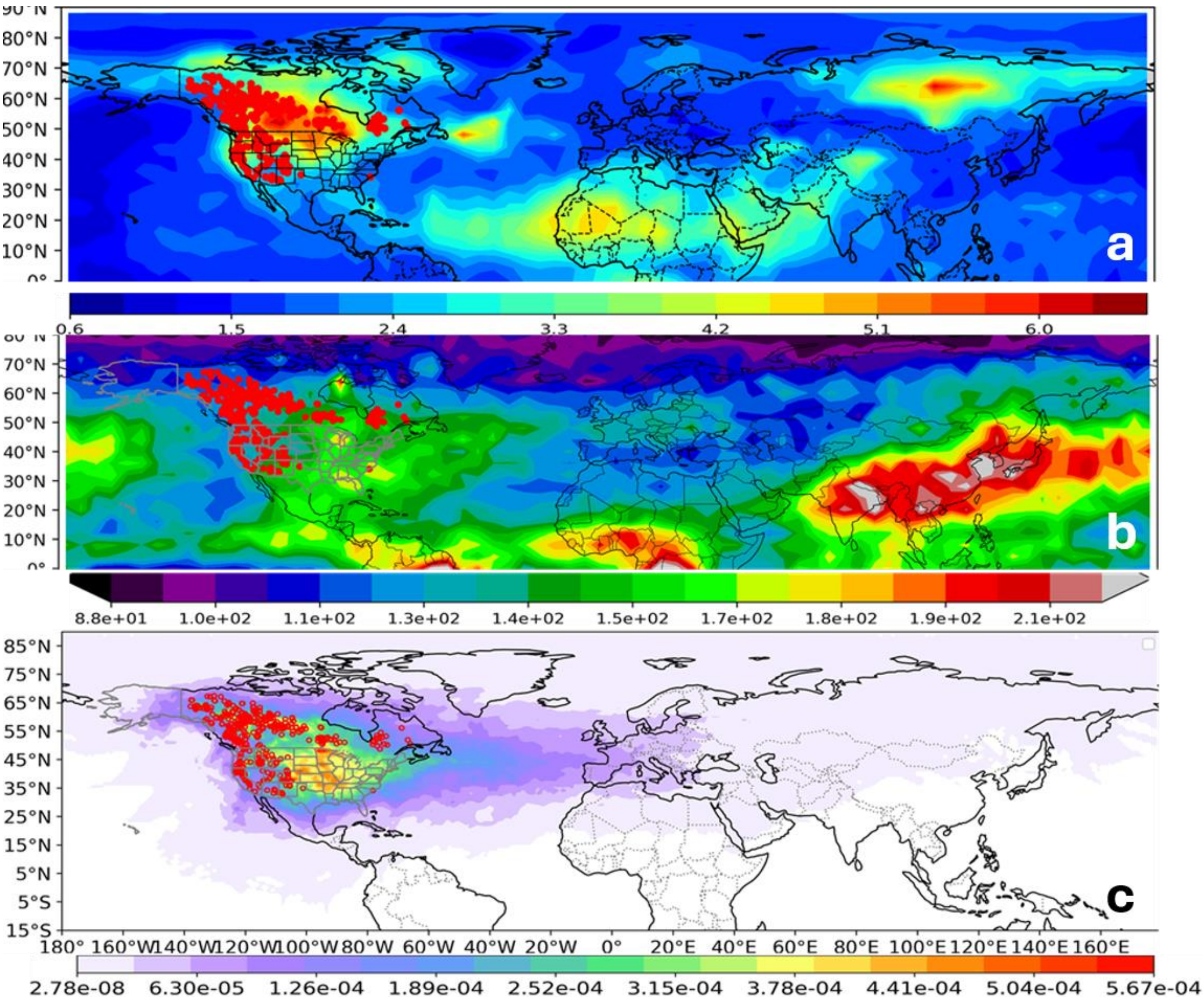

Figure 7. Comparison of (a) OMPS Aerosol Index (AI), (b) Aura MLS carbon monoxide (CO) concentrations, and (c) LaTM trajectory-based air parcel density maps during selected periods following pyroCb events. These panels highlight the spatial correspondence between satellite-observed aerosols, trace gas enhancements, and modeled smoke transport. The 99th percentiles of MLS-CO at 215 hPa and OMPS-AI were calculated over unique dates (948 days from 2013 to 2023) for the seven days following each event.

7 Operational Applications of Transport Diagnostics

Figure 8 shows the application of the transport pathways of the current study, which already support the community to plan, coordinate, and study pyroCbs. The top two figures show the PDF and age of the pyroCb plumes over North America between July, 27th to September, 9th constructed with all (115 in total) pyroCbs which took place between 2013 and 2023. This period coincides with the timings of the planned NASA INSPYRE mission to study pyroCbs over North America

https://doi.org/10.5194/egusphere-2026-3536
Preprint. Discussion started: 6 July 2026

(Peterson et al., 2025b). The plots highlight the ranges of the two aircrafts that will operate during the mission; one is ER-2 which will be based in Montana, and the other one the GV which will be based in Colorado. The circles show the ranges and the loiter times. The climatological pdf and age plots indicate the likelihood of sampling smoke layers in proximity to potential pyroCbs regions and associated with the likely age of the smoke. There are mainly three transport hotpots (smoke accumulation zones) approximately at (40°N, 120°W), (45°N, 110°W), and (35°N, 90°W) highlighting the higher probability of the smoke sampling, especially the fresh plumes. The average age of the smoke layers at the first two transport hotspots is less than 24 hours. Although most of the pyroCb locations are further northwest, the third transport hotspot of the downstream plume, has an average age less than 48 hours, enough to have more preparation to plan and sample the short- to mid-range plume at the downstream.

The bottom two contours in Fig. 8, represent the horizontal distribution of the global smoke layers (latitude vs longitude) and the vertical distribution of the smoke layers (altitude vs longitude). The vertical distribution plot is sampled within 45°N to 55° N, the latitude of the two stations of the BalNeO network (Vernier et al., 2025). The two white crosses and verticals lines represent the two locations, one at Minnesota, USA and another at Reims, France. The Minnesota station is great for short to mid-range sampling a pyroCb smoke layers, while the Reims station is great for long-range sampling. So, the two stations perfectly sit at the transport hotspot with the pyroCb concentrations. There have been already several samplings of the pyroCb smoke using the network.

Figure S8 shows aerosol concentration profiles from 3 flights conducted between 2022 and 2025 in Reims, Salina, and Minnesota. The flight on 06/03/25 conducted from Reims was planned with the trajectory forecast from LaTM of the pyroCb plume from the Red Earth East Complex Fire (REECF), one of the largest pyroCb of the 2025 season in North America. We sampled the REECF pyroCb plume reflected in the largest aerosol concentration ever measured by our system near the tropopause (700-800#/cm3). A near-source pyroCb plume was also detected on 06/17/22 during a balloon flight conducted from Salina/US (Fig. S8c) but with aerosol concentration significantly lower (up to 100#/cm3). Finally, a flight from Minnesota seems to have possibly crossed an aged pyroCb plume with aerosol concentration up to 7-8#/cm3 near 10 km on 08/27/25. The volumetric size distribution of smoke plumes from the 3 pyroCb plume significantly differs from background stratospheric aerosol with the presence of two aerosol modes, a mode of fine particles below 0.7 µm and a larger mode up to 2-3 µm. The mean radius mode of the fine mode is likely smaller than the lower size threshold of the POPC (0.3 µm). Overall, this work demonstrates the synergy between trajectory analysis and balloon measurements of pyroCb plumes.

A unique aspect of this study is the development of a decadal, pyroCb-specific trajectory climatology that quantifies preferred smoke-transport pathways across source regions, seasons, transport ages, and atmospheric layers. This scalable and customizable framework can inform aviation and mission planning by identifying routes and airspace sectors that are more prone to wildfire-smoke influence, including reduced visibility and potential encounters with pyroCb-related smoke layers, smoke-charged vortices, and turbulence. Specifically, the diagnostics quantify how interception probability varies with latitude, longitude, altitude, time since injection, season, source region, and vertical regime, as shown in Figs. 3–6, S5–S7, and S9–S10. Because the analysis can be subset by time window, regional domain, transport age, and altitude layer, it provides a flexible basis for targeted applications such as aircraft-route assessment, field-campaign planning, and interpretation of satellite-observed smoke signatures. The same framework also highlights corridors that are more susceptible to cross-tropopause transport (Fig. S6), where smoke can transition between the troposphere, UTLS, and lower stratosphere, increasing the likelihood of persistent layers near common flight altitudes (Khaykin, S. et al. 2025). These insights can support route and altitude adjustments during active fire periods, reduce the likelihood of traversing concentrated smoke plumes, and thereby mitigate risks to aircraft operations and engines. They may also provide useful context for post-flight assessment and operational interpretation by helping distinguish externally sourced wildfire smoke (e.g., odor or haze episodes) from onboard engine or cabin sources, potentially reducing unnecessary operational disruption, including precautionary diversions or emergency landings.

Because these maps represent a multi-event, pyroCb-conditioned climatology, the downwind pathway of any individual pyroCb plume may depart from the mean pattern depending on the synoptic steering at the time of injection; accordingly, the climatology is best used as a probabilistic guide for identifying likely transport corridors and downstream sampling/avoidance regions rather than as a deterministic prediction for a specific event.

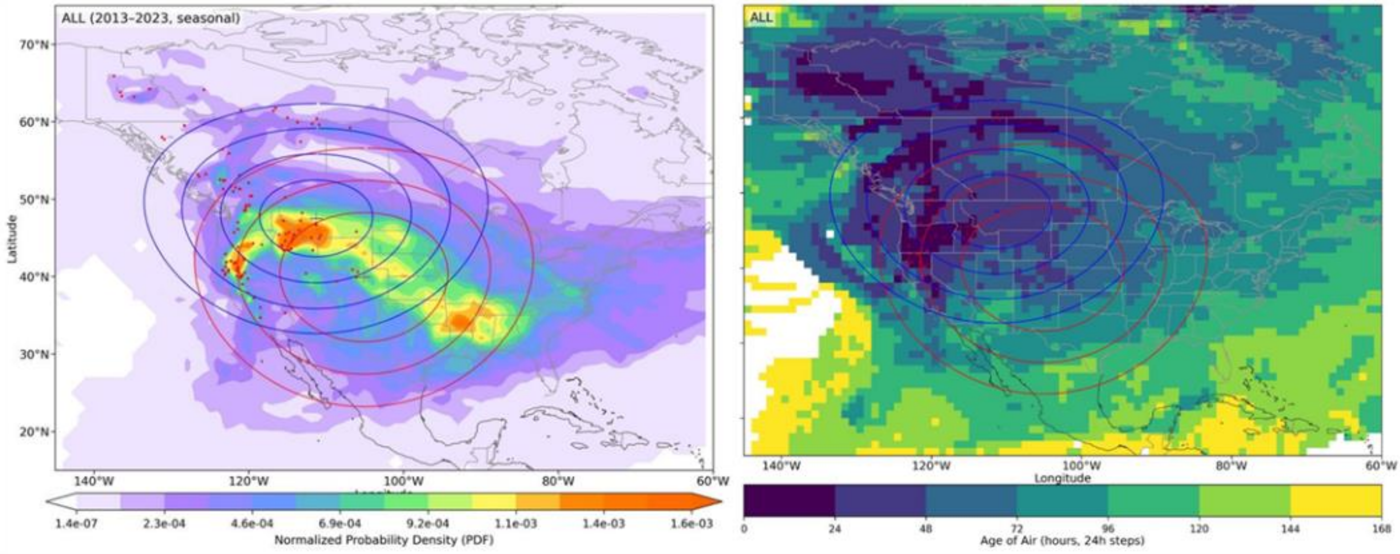

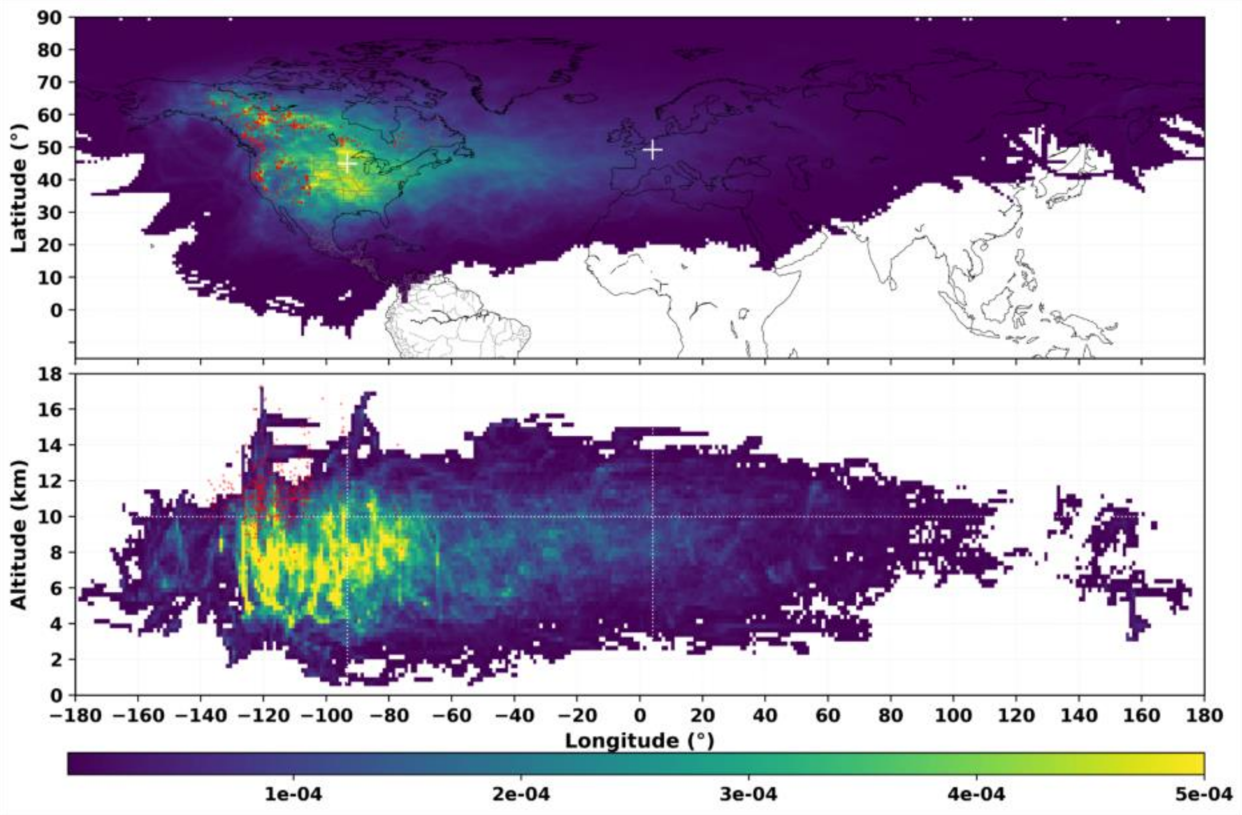

Figure 8. The top two panels show the probability density function (PDF) and average age of pyroCb smoke transport from July 27 to September 9 (corresponding to the INSPYRE mission period) during 2013–2023. Crosses indicate the locations of the two flight bases (Montana and Colorado) for the ER2 and GV aircraft, while circles denote flight ranges and loiter times. The bottom two panels display the global distribution of pyroCb smoke and its vertical distribution, the vertical plot being sampled within 45°N to 55°N; the white horizontal line marks the average tropopause height in this latitude band. The two crosses and two vertical lines indicate the locations of the BalNeO network sites in Minnesota, USA, and Reims, France. 540

545 8 Discussions

We study the North American pyroCb transport in a coherent framework, showing how these extreme fire-driven convection events spread across regions (United States and Canada) and through different atmospheric layers (troposphere, UTLS, stratosphere). We show that these transport patterns vary by season (spring, summer, and fall) and within targeted time windows relevant to pyroCb activity. Our interpretation is supported not only by transport-model diagnostics but also by 550 independent satellite observations and additional datasets, which increases confidence in the robustness of the findings. Within this framework, we identify the dominant transport pathways and highlight situations where the transport deviates from these typical routes. We then discuss the potential consequences of pyroCb-driven transport for atmospheric composition and impacts, including radiative effects and possible ozone-related changes. Finally, we outline how these insights can be used to improve model representation and forecasting and to support planning for future events and observations.

8.1 Synoptic Controls on PyroCb Smoke Transport

The transport analysis identifies several distinct aerosol anomalies that deviate from standard eastward zonal flow. Near the Yukon (60°N, 130°W), elevated smoke concentrations are observed to the west of the pyroCb injection points, a phenomenon known as retrograde transport (Fig. S10 (middle), Fig. 3). This westward displacement may reflect the influence of anomalous upper-level circulation, including cutoff-low or omega-blocking-type patterns, which can disrupt the typical eastward transport and redirect pyroCb smoke within the UTLS (Khaykin et al., 2025; Peterson et al., 2025a) (Fig. S10 (top)). Transport toward Hudson Bay, with occasional weak accumulation over or near the region, appears in other years and seasons in our trajectory diagnostics, mainly for higher-latitude Canadian pyroCb events. The pronounced fall maximum near 55° N, 85° W (Fig. 4c, Fig. S10(bottom)), however, is mainly amplified by the September 2023 Canadian pyroCb events and is most likely linked to late-season synoptic steering that directed Canadian smoke north-eastward into the Hudson Bay sector (Jain et al., 2024; Khaykin et al., 2025). The subtropical-Pacific pathway appears recurrent in summer (Fig. 4b), consistent with NAMA/subtropical-ridge control of high-altitude convective outflow toward Pacific-side export regions (Clapp et al., 2021). Its appearance in the fall composite near 20°–30° N, 120°–130° W is better interpreted as an episodic 2019–2020 anomaly (Fig. S11), with the 2020 contribution consistent with amplified upper-level ridging/Rossby-wave breaking (Russell et al., 2024) and long-range transport of upper-tropospheric western U.S. smoke (Ceamanos et al., 2023). The aerosol accumulation observed in the subtropics represents an aged plume that has undergone southward meridional transport. Upon reaching approximately 30°N, this stagnant air mass interacts with the Subtropical Jet (STJ), where it is entrained and rapidly accelerated eastward, transitioning from a blocking-dominated regime to a jet-driven zonal transport regime (Figs. S10 and S5). At lower tropical latitudes near the TTL, the easterly arrows in Figs. S5 and S10 may indicate westward transport by tropical easterly flow, potentially modulated by the QBO phase, suggesting a distinct tropical pathway separate from the dominant eastward subtropical and midlatitude transport.

The vertical contours of smoke age (Fig. 6) serve as a proxy for transport velocity, indicating the time required for smoke layers at different altitudes to reach a specific location. The data reveals that transport is most rapid in the upper troposphere, where high-velocity jet stream winds drive faster zonal advection compared to both the stratosphere and the lower troposphere. This vertical gradient supports critical inferences regarding residence time: while tropospheric layers are subject to rapid removal via precipitation, the stratosphere is characterized by high stability (stratification) and an absence of wet deposition. Consequently, stratospheric aerosols can only be removed through slow gravitational settling or large-scale Brewer-Dobson circulation, resulting in residence times ranging from months to years.

https://doi.org/10.5194/egusphere-2026-3536
Preprint. Discussion started: 6 July 2026

8.2 Tropical Reach and Cross-Hemispheric Export of North American pyroCb Smoke

We observe that North American pyroCb smoke can reach tropical latitudes and that a small fraction of trajectories show cross-equatorial excursions into the Southern Hemisphere (Figs. 3–6), consistent with prior evidence of PyroCb/UTLS smoke reaching low latitudes and tropical pathways (Fromm et al., 2019; Kloss et al., 2019, Das et al., 2021). However, this transport appears to be occasional and less dense. Several factors contribute to the low density (low PDF values) of this transport. One main reason is that we only tracked the trajectories for seven days, which is significantly shorter than the typical median tracking duration. Another contributing factor is the limited number of air parcels from individual events and the two-hour release window for sustained hours. To obtain more robust data on the transport of pyroCb smoke to the tropics and southern hemisphere, it would be beneficial to run trajectories for longer periods (weeks to months) and with a greater number of air parcels, while also allowing for longer sustained hours. Additionally, this transport phenomenon is dependent on spatiotemporal factors, as discussed in section 5.2. For the seven-day run, we observe that summer events and pyroCb smoke from the USA demonstrate this behaviour more (see Fig. 4b, e). The transport is more prominent within the same longitudinal band around 110°W where the pyroCb events originate. The altitude levels at which this transport occurs can be seen in Fig. 6 and Fig. S5. Some of these smoke layers may reach the stratosphere, as discussed in the earlier results section, which provides a detailed explanation of the transport mechanisms involved.

We also observe cases in which smoke from North American PyroCb events intrudes into the tropical–subtropical circulation associated with the Asian summer monsoon anticyclone (ASMA/AMA), similar to the pathway discussed by Kloss et al. (2019). In that study, TRACZILLA back-trajectories were typically integrated for 9 days, and were extended to 18 days for selected profiles to strengthen source attribution. Extending our forward-trajectory integrations beyond 7 days (e.g., toward ~9 days, and longer in sensitivity tests) would likely capture a more complete depiction of advection and possible entrainment along the ASMA boundary, improving our ability to diagnose this connection when it occurs.

8.3 Environmental Implications of Transport Diagnostics

Studying the transport of pyroCb plumes in the stratosphere is relevant for many science applications associated with assessing their radiative and climate impacts and their influence on stratospheric ozone chemistry. Large aerosols measured in smoke plume in 2022, 5 days after a pyroCb in New Mexico suggest that the radiative cooling could be larger than initially assumed (Li et al., 2025). Recent studies have found that stratospheric smoke has resulted in the loss of stratospheric ozone over the midlatitudes after the Australian New Year (ANY) pyroCb event (Bernath et al., 2022; Solomon et al., 2022) and could delay future ozone recovery. The pyroCb plume database that is developed in this study can help assess the radiative, climate, and stratospheric ozone impacts of pyroCbs, a growing phenomenon affecting the stratosphere.

In addition, the mid-range transport of pyroCb plumes in this study suggest that these plumes return to the troposphere where they can impact weather (especially on the downstream smoke accumulation regions) since aerosol can serve as CCN and thus affect cloud formation. While travelling back to the troposphere, they could have an impact on Air quality away from the fires. In addition, smoke plumes can reduce solar radiation near the ground and lower solar energy production (Corwin et al., 2025).

The transport of smoke plumes from North America across the Atlantic has the potential to influence cirrus cloud formation over the North Atlantic region, Europe, and the Arctic Circle. Evidence of cirrus cloud formation triggered by aged smoke plumes from the 2020 California wildfires has been observed by Mamouri et al. (2023) through routine ground-based lidar and radiosonde measurements. Synergistic observations using Mie-Raman and fluorescence lidars have also detected aged smoke within cirrus cloud layers over France (Veselovskii et al., 2022). In situ measurements of black carbon from IAGOS-CARRIBIC have revealed high concentrations of black carbon, with thick coatings, in the lowermost stratosphere over North America and the North Atlantic region (Ditas et al., 2019) which may potentially influence cirrus cloud formation. This may lead to local radiative heating and could significantly influence regional radiative forcing. Additionally, these smoke plumes may affect Arctic cirrus formation, as observed from ship-borne measurements in the Arctic (Ansmann et al., 2025).

Although the present analysis focuses specifically on North American pyroCb events, the resulting transport patterns—particularly those diagnosed in the tropospheric layers—also provide insight into regions potentially exposed to wildfire-related air pollution. Because pyroCbs represent intense wildfire events capable of injecting smoke into both the upper troposphere/lower stratosphere and lower atmospheric layers, the tropospheric trajectory PDFs can be interpreted as a useful proxy for identifying likely downwind transport pathways and receptor regions affected by broader wildfire smoke and boundary-layer pollution.

The LaTM trajectory PDF represents the relative frequency or residence of ensemble trajectory points within each grid cell. By itself, this field is not a mass-conserving aerosol concentration product. However, because the trajectories were initialized from pyroCb smoke source regions and the regions of enhanced PDF were independently corroborated by OMPS Aerosol Index and MLS CO enhancements, we interpret the PDF as a relative proxy for likely smoke loading/concentration. Thus, the PDF is used here both as a transport diagnostic and as an observationally supported indicator of regions where pyroCb smoke was more likely to be concentrated.

8.4 Potential ENSO Influence on the Seasonal and Regional Distribution of PyroCbs

Large-scale climate variability, including ENSO, may contribute to year-to-year and regional variability in pyroCb activity (Peterson et al., 2025a). Using the ENSO 3.4 index (Huang et al., 2019), we explored how seasonal and regional pyroCb occurrence varies with ENSO phase (Fig. S2). The results suggest that El Niño is associated with relatively more high-latitude pyroCbs over Canada (Luo, B. et al. 2025), whereas La Niña is associated with relatively lower-latitude pyroCbs over the USA (Keeping et al., 2025). Neutral conditions also appear to favour slightly higher-latitude than lower-latitude events. Overall, El Niño and neutral conditions are associated with more pyroCbs across North America in our dataset, with El Niño showing the highest frequencies. In contrast, ENSO does not appear to exert a strong influence on the longitudinal distribution of pyroCb occurrence, although El Niño (Luo, B. et al. 2025) and neutral conditions show a slight tendency toward more easterly events. These relationships should be interpreted cautiously, because ENSO influences may be delayed

https://doi.org/10.5194/egusphere-2026-3536
Preprint. Discussion started: 6 July 2026

and regionally dependent, operating through changes in large-scale circulation, precipitation, and land-surface moisture rather than through a simple direct cause-and-effect pathway. Thus, our results are best viewed as suggestive of a possible ENSO influence on pyroCb occurrence, while more quantitative analysis is needed to test the robustness of these patterns. Future studies will examine these relationships in greater detail, including the roles of precipitation, land-surface moisture, and other relevant meteorological controls. Any ENSO influence on pyroCb smoke transport is also likely indirect, through its modulation of pyroCb occurrence and location, whereas the actual transport pathways are controlled more directly by the contemporaneous meteorological environment.

9. Conclusion:

This study investigated transport of smoke plumes injected into the UTLS by pyroCb activity in North American during 2013–2023 using a worldwide pyroCb inventory (Peterson et al. 2025a), the NASA Langley Trajectory Model (Pierce and Fairlie, 1993), and MERRA-2 meteorological fields (Gelaro et al., 2017). The Chuckegg Creek pyroCb event demonstrated that LaTM can reproduce major observed transport features when compared with CALIPSO and OMPS, supporting its use for broader climatological analysis of pyroCb smoke pathways.

The climatological results show that pyroCb smoke transport over North America depends strongly on source region, season, injection altitude, vertical regime (Troposphere, UTLS, and Stratosphere), and synoptic meteorological setting. Short-range transport is characterized by fresh plume hotspots (accumulation zones) near northwestern Canada and the west-central United States, while the central United States acts as a downstream accumulation region where persistent smoke layers can develop, especially in the troposphere. Long-range transport is dominated by Canadian pyroCbs and frequently follows a trans-Atlantic pathway near 45° N, with smoke layers commonly located at UTLS altitudes of approximately 10–11 km after 4-5 days of transport.

Vertical-regime analysis further shows that pyroCb smoke is distributed across the troposphere, UTLS, and lower stratosphere. Tropospheric smoke is more concentrated near 30° N during short- to mid-range transport, before shifting toward the midlatitude pathway during longer-range export. UTLS smoke, dominated by Canadian pyroCbs, extends over a broad latitude range from about 30° N to 75° N and is centered near the 45° N pathway toward Europe. Stratospheric smoke transport occurs mainly between 35° N and 65° N, with the highest concentration near 50° N, and some smoke reaches approximately 6–7 km above the tropopause, are contributed by extreme events. These results indicate that pyroCb events can inject smoke into dynamically distinct atmospheric layers and that the subsequent transport is organized by both source location and large-scale circulation.

Seasonal differences are also important. Summer accounts for the largest number of pyroCb events and affects both Canadian and U.S. source regions, although Canadian events are more frequent. Canadian summer smoke often moves southward before following the midlatitude pathway toward Europe, whereas U.S. smoke more often follows a lower-latitude pathway near 30° N during short- and mid-range transport before also merging with the broader 40°–45° N export corridor. Spring events over Canada tend to follow more northerly pathways influenced by polar or midlatitude jets. Fall events over the United States show distinct transport behaviour, including transport by westerlies, interaction with the subtropical jet, enhanced smoke near Hudson Bay, and a convergence feature near 20°–30° N and 120°–130° W that can redirect smoke southward toward Mexico and westward over the Pacific Ocean.

The analysis also highlights the role of synoptic-scale circulation in shaping smoke pathways. Retrograde (westward) transport at high latitudes is likely linked to an Omega-blocking pattern, while enhanced smoke near Hudson Bay suggests that persistent regional circulation features can favour smoke accumulation far downstream of source regions. These findings show that pyroCb smoke transport cannot be explained by injection height alone; it also depends on the evolving meteorological environment into which the smoke is injected.

In addition to midlatitude and trans-Atlantic transport, the results show that North American pyroCb smoke can reach the tropics and, in some cases, cross into the Southern Hemisphere. This tropical and cross-hemispheric pathway occurs especially from U.S. pyroCbs during summer and follows a longitudinal band near the source region around 110° W. Smoke reaching the tropics is often located above 15 km and ascends through the tropical UTLS, indicating a potential pathway for longer-lived high-altitude transport. The Asian Summer Monsoon Anticyclone also appears to contribute to the tropical reach of some smoke layers. However, trajectory simulations extending beyond the current 7-day window are required to better characterize the long-range transport, residence time, and eventual redistribution of these plumes.

Independent satellite observations provide additional support for the major trajectory-based transport pathways. OMPS aerosol index signatures are located somewhat north of the LaTM probability-density fields during short-range transport, while MLS CO enhancements are located somewhat further south. However, both satellite tracers show reasonable agreement with LaTM in the mid-range hotspots and in the long-range pathway near 50° N. This agreement increases confidence that the trajectory diagnostics capture the dominant smoke-transport corridors, while the offsets among LaTM, OMPS-AI, and MLS-CO reflect differences in tracer sensitivity, sampling, vertical structure, and plume evolution.

The transport diagnostics also have practical value for mission planning, environmental interpretation, and operational assessment. The climatological hotspots support the placement and use of observation networks and campaigns such as BalNeO and INSPYRE, including short- and mid-range sampling near Minnesota and long-range trans-Atlantic sampling near Reims. The same diagnostics can help identify aviation routes more susceptible to smoke layers and regions where chemical, radiative, cloud-related, ozone-related, or dynamical impacts may be more likely. The seasonal and regional dependence of pyroCb frequency, including its relationship with the ONI ENSO index, further suggests that large-scale climate variability may influence not only pyroCb occurrence but also the preferred transport pathways of the resulting smoke.

Overall, this study provides a scalable framework for understanding how wildfire-driven convective injections redistribute smoke from regional source areas to continental, trans-Atlantic, tropical, and potentially hemispheric scales. By combining trajectory modelling, vertical-regime analysis, seasonal and synoptic interpretation, and multi-sensor satellite corroboration, the results show that North American pyroCbs can affect atmospheric chemical, radiative, and dynamical conditions from the troposphere to the lower stratosphere far downwind.

Code and data availability

The publicly available satellite and reanalysis datasets used in this study are cited in the text. The processed LaTM trajectory outputs, derived data products, and analysis scripts are available from the corresponding author upon reasonable request.

Author contributions

RCD and JPV conceptualized the study. RCD curated the datasets, developed the methodology and software workflow, performed the formal analysis and validation, investigated the results, prepared the visualizations, and wrote the original manuscript draft. JPV contributed to the methodology, project administration, supervision, and interpretation of the results. JPV and DAP contributed to funding acquisition. AKP, ND, LJ, and JF collected and provided the balloon observations, and JPV analyzed the balloon data. JPV, AKP, DAP, MF, GK, ND, LJ, and JF contributed scientific feedback and manuscript review. All authors reviewed and approved the final manuscript.

Competing interests

The authors declare that they have no conflict of interest.

Acknowledgements

We thank the SAGE III/ISS, OMPS, MLS, MERRA-2, and balloon-campaign teams for providing the datasets and resources used in this study. We also thank Hyun-Deok Choi and Murali Natarajan for helpful discussions on LaTM trajectory analyses. AI tools have been used to improve parts of the manuscript's phrasing. We would like to express our gratitude to the NIA administrative team for their support, including Carly Bosco, Susan Sorlie, Nicole Burns, Rita Aguillard, and Lara

Hawthorne. Additionally, we acknowledge Guoqing Shen from Coherent Applications Inc. and Johnny Mau from NASA Langley for their assistance with the balloon launching.

Financial support

Support for this work was provided by NASA's INjected Smoke and PYRocumulonimbus Experiment (INSPYRE), the NASA SAGE III/ISS program, the NASA Upper Atmospheric Composition Observation program, and the U.S. Naval Research Laboratory's 6.2 Base Program.

References

Fromm, M., Servranckx, R., Stocks, B. J., and Peterson, D. A.: Understanding the critical elements of the pyrocumulonimbus storm sparked by high-intensity wildland fire, Communications Earth & Environment, 3, https://doi.org/10.1038/s43247-022-00566-8, 2022.

Peterson, D. A., Berman, M. T., Fromm, M. D., Servranckx, R., Julstrom, W. J., Hyer, E. J., Campbell, J. R., McHardy, T. M., and Lambert, A.: Worldwide inventory reveals the frequency and variability of pyrocumulonimbus and stratospheric smoke plumes during 2013–2023, Npj Climate and Atmospheric Science, 8, https://doi.org/10.1038/s41612-025-01188-5, 2025.

Khaykin, S., Bekki, S., Godin-Beekmann, S., Fromm, M. D., Goloub, P., Hu, Q., Josse, B., Laeng, A., Meziane, M., Peterson, D. A., Pelletier, S., and Thouret, V.: Stratospheric impact of the anomalous 2023 Canadian wildfires: the two vertical pathways of smoke, Atmospheric Chemistry and Physics, 25, 14551–14571, https://doi.org/10.5194/acp-25-14551-2025, 2025.

Jain, P., Barber, Q. E., Taylor, S. W., Whitman, E., Acuna, D. C., Boulanger, Y., Chavardès, R. D., Chen, J., Englefield, P., Flannigan, M., Girardin, M. P., Hanes, C. C., Little, J., Morrison, K., Skakun, R. S., Thompson, D. K., Wang, X., and Parisien, M.-A.: Drivers and impacts of the Record-Breaking 2023 wildfire season in Canada, Nature Communications, 15, 6764, https://doi.org/10.1038/s41467-024-51154-7, 2024b.

Li, X., Mann, M. E., Wehner, M. F., and Christiansen, S.: Increased frequency of planetary wave resonance events over the past half-century, Proceedings of the National Academy of Sciences, 122, e2504482122, https://doi.org/10.1073/pnas.2504482122, 2025.

Peterson, D. A., Campbell, J. R., Hyer, E. J., Fromm, M. D., Kablick, G. P., Cossuth, J. H., and DeLand, M. T.: Wildfire-driven thunderstorms cause a volcano-like stratospheric injection of smoke, Npj Climate and Atmospheric Science, 1, https://doi.org/10.1038/s41612-018-0039-3, 2018.

Fromm, M., Bevilacqua, R., Servranckx, R., Rosen, J., Thayer, J. P., Herman, J., and Larko, D.: Correction to "Pyro-cumulonimbus injection of smoke to the stratosphere: Observations and impact of a super blowup in northwestern Canada on 3–4 August 1998," Journal of Geophysical Research Atmospheres, 110, https://doi.org/10.1029/2005jd006171, 2005.

Fromm, M., Lindsey, D. T., Servranckx, R., Yue, G., Trickl, T., Sica, R., Doucet, P., and Godin-Beekmann, S.: The untold story of Pyrocumulonimbus, Bulletin of the American Meteorological Society, 91, 1193–1210, https://doi.org/10.1175/2010bams3004.1, 2010.

Das, S., Colarco, P. R., Oman, L. D., Taha, G., and Torres, O.: The long-term transport and radiative impacts of the 2017 British Columbia pyrocumulonimbus smoke aerosols in the stratosphere, Atmospheric Chemistry and Physics, 21, 12069–12090, https://doi.org/10.5194/acp-21-12069-2021, 2021b.

Katich, J. M., Apel, E. C., Bourgeois, I., Brock, C. A., Bui, T. P., Campuzano-Jost, P., Commane, R., Daube, B., Dollner, M., Fromm, M., Froyd, K. D., Hills, A. J., Hornbrook, R. S., Jimenez, J. L., Kupc, A., Lamb, K. D., McKain, K., Moore, F., Murphy, D. M., Nault, B. A., Peischl, J., Perring, A. E., Peterson, D. A., Ray, E. A., Rosenlof, K. H., Ryerson, T., Schill, G. P., Schroder, J. C., Weinzierl, B., Thompson, C., Williamson, C. J., Wofsy, S. C., Yu, P., and Schwarz, J. P.: Pyrocumulonimbus affect average stratospheric aerosol composition, Science, 379, 815–820, https://doi.org/10.1126/science.add3101, 2023.

Bernath, P., Boone, C., and Crouse, J.: Wildfire smoke destroys stratospheric ozone, Science, 375, 1292–1295, https://doi.org/10.1126/science.abm5611, 2022.

Solomon, S., Dube, K., Stone, K., Yu, P., Kinnison, D., Toon, O. B., Strahan, S. E., Rosenlof, K. H., Portmann, R., Davis, S., Randel, W., Bernath, P., Boone, C., Bardeen, C. G., Bourassa, A., Zawada, D., and Degenstein, D.: On the stratospheric chemistry of midlatitude wildfire smoke, Proceedings of the National Academy of Sciences, 119, e2117325119, https://doi.org/10.1073/pnas.2117325119, 2022.

Peterson, D. A., Fromm, M. D., McRae, R. H. D., Campbell, J. R., Hyer, E. J., Taha, G., Camacho, C. P., Kablick, G. P., Schmidt, C. C., and DeLand, M. T.: Australia's Black Summer pyrocumulonimbus super outbreak reveals potential for increasingly extreme stratospheric smoke events, Npj Climate and Atmospheric Science, 4, https://doi.org/10.1038/s41612-021-00192-9, 2021.

Khaykin, S., Legras, B., Bucci, S., Sellitto, P., Isaksen, L., Tencé, F., Bekki, S., Bourassa, A., Rieger, L., Zawada, D., Jumelet, J., and Godin-Beekmann, S.: The 2019/20 Australian wildfires generated a persistent smoke-charged vortex rising up to 35 km altitude, Communications Earth & Environment, 1, https://doi.org/10.1038/s43247-020-00022-5, 2020b.

Kablick, G. P., Allen, D. R., Fromm, M. D., and Nedoluha, G. E.: Australian PyroCB smoke generates Synoptic-Scale stratospheric anticyclones, Geophysical Research Letters, 47, https://doi.org/10.1029/2020gl088101, 2020b.

Zhang, S., Solomon, S., Boone, C. D., and Taha, G.: Investigating the vertical extent of the 2023 summer Canadian wildfire impacts with satellite observations, Atmospheric Chemistry and Physics, 24, 11727–11736, https://doi.org/10.5194/acp-24-11727-2024, 2024.

Khaykin, S. M., Godin-Beekmann, S., Hauchecorne, A., Pelon, J., Ravetta, F., and Keckhut, P.: Stratospheric smoke with unprecedentedly high backscatter observed by Lidars above southern France, Geophysical Research Letters, 45, 1639–1646, https://doi.org/10.1002/2017gl076763, 2018.

Butchart, N.: The Brewer-Dobson circulation, Reviews of Geophysics, 52, 157–184, https://doi.org/10.1002/2013rg000448, 2014.

Kloss, C., Berthet, G., Sellitto, P., Ploeger, F., Bucci, S., Khaykin, S., Jégou, F., Taha, G., Thomason, L. W., Barret, B., Flochmoen, E. L., Von Hobe, M., Bossolasco, A., Bègue, N., and Legras, B.: Transport of the 2017 Canadian wildfire plume to the tropics via the Asian monsoon circulation, Atmospheric Chemistry and Physics, 19, 13547–13567, https://doi.org/10.5194/acp-19-13547-2019, 2019.

Osborne, M. J., De Leeuw, J., Witham, C., Schmidt, A., Beckett, F., Kristiansen, N., Buxmann, J., Saint, C., Welton, E. J., Fochesatto, J., Gomes, A. R., Bundke, U., Petzold, A., Marenco, F., and Haywood, J.: The 2019 Raikoke volcanic eruption – Part 2: Particle-phase dispersion and concurrent wildfire smoke emissions, Atmospheric Chemistry and Physics, 22, 2975–2997, https://doi.org/10.5194/acp-22-2975-2022, 2022.

Yu, P., Toon, O. B., Bardeen, C. G., Zhu, Y., Rosenlof, K. H., Portmann, R. W., Thornberry, T. D., Gao, R.-S., Davis, S. M., Wolf, E. T., De Gouw, J., Peterson, D. A., Fromm, M. D., and Robock, A.: Black carbon lofts wildfire smoke high into the stratosphere to form a persistent plume, Science, 365, 587–590, https://doi.org/10.1126/science.aax1748, 2019b.

Allen, D. R., Fromm, M. D., Kablick, G. P., III, and Nedoluha, G. E.: Smoke with Induced Rotation and Lofting (SWIRL) in the Stratosphere, Journal of the Atmospheric Sciences, 77, 4297–4316, https://doi.org/10.1175/jas-d-20-0131.1, 2020.

Pierce, R. B. and Fairlie, T. D. A.: Chaotic advection in the stratosphere: Implications for the dispersal of chemically perturbed air from the polar vortex, Journal of Geophysical Research Atmospheres, 98, 18589–18595, https://doi.org/10.1029/93jd01619, 1993b.

Vernier, J. -p., Fairlie, T. D., Deshler, T., Ratnam, M. V., Gadhavi, H., Kumar, B. S., Natarajan, M., Pandit, A. K., Raj, S. T. A., Kumar, A. H., Jayaraman, A., Singh, A. K., Rastogi, N., Sinha, P. R., Kumar, S., Tiwari, S., Wegner, T., Baker, N., Vignelles, D., Stenchikov, G., Shevchenko, I., Smith, J., Bedka, K., Kesarkar, A., Singh, V., Bhate, J., Ravikiran, V., Rao, M. D., Ravindrababu, S., Patel, A., Vernier, H., Wienhold, F. G., Liu, H., Knepp, T. N., Thomason, L., Crawford, J., Ziemba, L., Moore, J., Crumeyrolle, S., Williamson, M., Berthet, G., Jégou, F., and Renard, J. -b.: BATAL: The balloon measurement campaigns of the Asian Tropopause aerosol layer, Bulletin of the American Meteorological Society, 99, 955–973, https://doi.org/10.1175/bams-d-17-0014.1, 2017b.

Vernier, H., Rastogi, N., Liu, H., Pandit, A. K., Bedka, K., Patel, A., Ratnam, M. V., Kumar, B. S., Zhang, B., Gadhavi, H., Wienhold, F., Berthet, G., and Vernier, J.-P.: Exploring the inorganic composition of the Asian Tropopause Aerosol Layer using medium-duration balloon flights, Atmospheric Chemistry and Physics, 22, 12675–12694, https://doi.org/10.5194/acp-22-12675-2022, 2022b.

Pandit, A. K., Vernier, J.-P., Fairlie, T. D., Bedka, K. M., Avery, M. A., Gadhavi, H., Ratnam, M. V., Dwivedi, S., Jyothi, K. A., Wienhold, F. G., Vömel, H., Liu, H., Zhang, B., Kumar, B. S., Dinh, T., and Jayaraman, A.: Investigating the role of typhoon-induced waves and stratospheric hydration in the formation of tropopause cirrus clouds observed during the 2017 Asian monsoon, Atmospheric Chemistry and Physics, 24, 14209–14238, https://doi.org/10.5194/acp-24-14209-2024, 2024b.

Vernier, J. -p., Fairlie, T. D., Murray, J. J., Tupper, A., Trepte, C., Winker, D., Pelon, J., Garnier, A., Jumelet, J., Pavolonis, M., Omar, A. H., and Powell, K. A.: An advanced system to monitor the 3D structure of diffuse volcanic ash clouds, Journal of Applied Meteorology and Climatology, 52, 2125–2138, https://doi.org/10.1175/jamc-d-12-0279.1, 2013b.

Fairlie, T. D., Vernier, J. -p., Natarajan, M., and Bedka, K. M.: Dispersion of the Nabro volcanic plume and its relation to the Asian summer monsoon, Atmospheric Chemistry and Physics, 14, 7045–7057, https://doi.org/10.5194/acp-14-7045-2014, 2014b.

Soja, A. J., Fairlie, T. D., Westberg, D., and Pouliot, G.: Biomass burning plume injection height using CALIOP, MODIS and the NASA Langley Trajectory Model, 2012 US EPA International Emission Inventory Conference, available at: https://www3.epa.gov/ttnchie1/conference/ei20/session7/asoja.pdf, last access: 15 June 2026, 2012.

Choi, H. G., Vernier, J.-P., Fairlie, T. D., Natarajan, M., and Liu, H.: Assessing the radiative impact of the 2019–2020 Australian bushfires using trajectory-mapped CALIPSO observations, NASA Technical Reports Server (NTRS), available at: https://ntrs.nasa.gov/citations/20205005144, last access: 15 June 2026, 2020.

Winker, D. M., Vaughan, M. A., Omar, A., Hu, Y., Powell, K. A., Liu, Z., Hunt, W. H., and Young, S. A.: Overview of the CALIPSO mission and CALIOP data processing algorithms, Journal of Atmospheric and Oceanic Technology, 26, 2310–2323, https://doi.org/10.1175/2009jtecha1281.1, 2009b.

Torres, O. O.: OMPS-NPP L2 NM Aerosol Index swath orbital, https://doi.org/10.5067/40l92g8144iv, 2019.

Schwartz, M., Pumphrey, H., Livesey, N., Read, W., and Fuller, R.: MLS/AURA Level 3 daily binned carbon monoxide (CO) mixing ratio on assorted grids V005, https://doi.org/10.5067/aura/mls/data/3506, 2021.

Gelaro, R., McCarty, W., Suárez, M. J., Todling, R., Molod, A., Takacs, L., Randles, C. A., Darmenov, A., Bosilovich, M. G., Reichle, R., Wargan, K., Coy, L., Cullather, R., Draper, C., Akella, S., Buchard, V., Conaty, A., Da Silva, A. M., Gu, W., Kim, G.-K., Koster, R., Lucchesi, R., Merkova, D., Nielsen, J. E., Partyka, G., Pawson, S., Putman, W., Rienecker, M., Schubert, S. D., Sienkiewicz, M., and Zhao, B.: The Modern-Era Retrospective Analysis for Research and Applications, Version 2 (MERRA-2), Journal of Climate, 30, 5419–5454, https://doi.org/10.1175/jcli-d-16-0758.1, 2017.

Hoffmann, L. and Spang, R.: An assessment of tropopause characteristics of the ERA5 and ERA-Interim meteorological reanalyses, Atmospheric Chemistry and Physics, 22, 4019–4046, https://doi.org/10.5194/acp-22-4019-2022, 2022.

Fromm, M. D., Kablick, G. P., Peterson, D. A., Kahn, R. A., Flower, V. J. B., and Seftor, C. J.: Quantifying the source term and uniqueness of the August 12, 2017 Pacific Northwest PyrOCB event, Journal of Geophysical Research Atmospheres, 126, https://doi.org/10.1029/2021jd034928, 2021b.

Kim, M.-H., Omar, A. H., Tackett, J. L., Vaughan, M. A., Winker, D. M., Trepte, C. R., Hu, Y., Liu, Z., Poole, L. R., Pitts, M. C., Kar, J., and Magill, B. E.: The CALIPSO version 4 automated aerosol classification and lidar ratio selection algorithm, Atmospheric Measurement Techniques, 11, 6107–6135, https://doi.org/10.5194/amt-11-6107-2018, 2018.

Fromm, M., Torres, O., Diner, D., Lindsey, D., Hull, B. V., Servranckx, R., Shettle, E. P., and Li, Z.: Stratospheric impact of the Chisholm pyrocumulonimbus eruption: 1. Earth-viewing satellite perspective, Journal of Geophysical Research Atmospheres, 113, https://doi.org/10.1029/2007jd009153, 2008b.

Fu, Q., Hu, Y., and Yang, Q.: Identifying the top of the tropical tropopause layer from vertical mass flux analysis and CALIPSO lidar cloud observations, Geophysical Research Letters, 34, https://doi.org/10.1029/2007gl030099, 2007.

Fromm, M., Peterson, D., and Di Girolamo, L.: The primary convective pathway for observed wildfire emissions in the upper troposphere and lower stratosphere: a targeted reinterpretation, Journal of Geophysical Research Atmospheres, 124, 13254–13272, https://doi.org/10.1029/2019jd031006, 2019b.

Peterson, D. A., Lareau, N., and Kalashnikova, O. V.: The INjected Smoke and PYRocumulonimbus Experiment (INSPYRE), AGU25, available at: https://agu.confex.com/agu/agu25/meetingapp.cgi/Paper/1925825, last access: 15 June 2026, 2025.

Vernier, J.-P., Dumelié, N., Pandit, A. K., Souza, G., Flaten, J., Kiran, V. R., Das, R. C., Vernier, H., Joly, L., Quintao, D., Biazon, B., Ratnam, M. V., Rao, T. V., Rastogi, N., Berthet, G., Benoit, R., Dagaut, P., Grosselin, B., Landulfo, E., Liu, H., Fromm, M., Peterson, D., Wienhold, F., Kovilakam, M., Fadnavis, S., Abiodun, B., Xia, L., and Aboutanios, E.: The Balloon Network for Stratospheric Aerosol Observations (BalNeO), manuscript under review for Bull. Am. Meteorol. Soc., BAMS-D-25-0046, 2025.

Clapp, C. E., Smith, J. B., Bedka, K. M., and Anderson, J. G.: Identifying outflow regions of North American monsoon Anticyclone-Mediated meridional transport of convectively influenced air masses in the lower stratosphere, Journal of Geophysical Research Atmospheres, 126, e2021JD034644, https://doi.org/10.1029/2021jd034644, 2021b.

Russell, E. N., Loikith, P. C., Ajibade, I., Done, J. M., and Lower, C.: The meteorology and impacts of the September 2020 Western United States extreme weather event, Weather and Climate Extremes, 43, 100647, https://doi.org/10.1016/j.wace.2024.100647, 2024b.

Ceamanos, X., Coopman, Q., George, M., Riedi, J., Parrington, M., and Clerbaux, C.: Remote sensing and model analysis of biomass burning smoke transported across the Atlantic during the 2020 Western US wildfire season, Scientific Reports, 13, 16014, https://doi.org/10.1038/s41598-023-39312-1, 2023b.

Li, Y., Dykema, J. A., Peterson, D. A., Feng, X., Shen, X., June, N. A., Fromm, M. D., McHardy, T. M., Jacquot, J. L., Pittman, J. V., Daube, B. C., Wofsy, S. C., Dean-Day, J., Rapp, A. D., Bowman, K. P., Cziczo, D. J., Mickley, L. J., Pierce, J. R., and Keutsch, F. N.: Enhanced radiative cooling by large aerosol particles from wildfire-driven thunderstorms, Science Advances, 11, eadw6526, https://doi.org/10.1126/sciadv.adw6526, 2025b.

Corwin, K. A., Burkhardt, J., Corr, C. A., Stackhouse, P. W., Munshi, A., and Fischer, E. V.: Solar energy resource availability under extreme and historical wildfire smoke conditions, Nature Communications, 16, 245, https://doi.org/10.1038/s41467-024-54163-8, 2025b.

Mamouri, R.-E., Ansmann, A., Ohneiser, K., Knopf, D. A., Nisantzi, A., Bühl, J., Engelmann, R., Skupin, A., Seifert, P., Baars, H., Ene, D., Wandinger, U., and Hadjimitsis, D.: Wildfire smoke triggers cirrus formation: lidar observations over the eastern Mediterranean, Atmospheric Chemistry and Physics, 23, 14097–14114, https://doi.org/10.5194/acp-23-14097-2023, 2023.

Veselovskii, I., Hu, Q., Ansmann, A., Goloub, P., Podvin, T., and Korenskiy, M.: Fluorescence lidar observations of wildfire smoke inside cirrus: a contribution to smoke–cirrus interaction research, Atmospheric Chemistry and Physics, 22, 5209–5221, https://doi.org/10.5194/acp-22-5209-2022, 2022.

Ditas, J., Ma, N., Zhang, Y., Assmann, D., Neumaier, M., Riede, H., Karu, E., Williams, J., Scharffe, D., Wang, Q., Saturno, J., Schwarz, J. P., Katich, J. M., McMeeking, G. R., Zahn, A., Hermann, M., Brenninkmeijer, C. a. M., Andreae, M. O., Pöschl, U., Su, H., and Cheng, Y.: Strong impact of wildfires on the abundance and aging of black carbon in the lowermost stratosphere, Proceedings of the National Academy of Sciences, 115, E11595–E11603, https://doi.org/10.1073/pnas.1806868115, 2018b.

Ansmann, A., Jimenez, C., Roschke, J., Bühl, J., Ohneiser, K., Engelmann, R., Radenz, M., Griesche, H., Hofer, J., Althausen, D., Knopf, D. A., Dahlke, S., Gaudek, T., Seifert, P., and Wandinger, U.: Impact of wildfire smoke on Arctic cirrus formation – Part 1: Analysis of MOSAiC 2019–2020 observations, Atmospheric Chemistry and Physics, 25, 4847–4866, https://doi.org/10.5194/acp-25-4847-2025, 2025.

Huang, B., Thorne, P. W., Banzon, V. F., Boyer, T., Chepurin, G., Lawrimore, J. H., Menne, M. J., Smith, T. M., Vose, R. S., and Zhang, H.-M.: Extended Reconstructed Sea Surface Temperature, Version 5 (ERSSTV5): Upgrades, validations, and intercomparisons, Journal of Climate, 30, 8179–8205, https://doi.org/10.1175/jcli-d-16-0836.1, 2017.

Luo, B., Xiao, C., Luo, D., Fu, Q., Chen, D., Zhang, Q., Ge, Y., and Diao, Y.: Atmospheric and oceanic drivers behind the 2023 Canadian wildfires, Communications Earth & Environment, 6, https://doi.org/10.1038/s43247-025-02387-x, 2025.

Keeping, T. R., Shepherd, T. G., Prentice, I. C., Van Der Wiel, K., and Harrison, S. P.: Influence of global climate modes on wildfire occurrence in the contiguous United States under recent and future climates, Climate Dynamics, 64, 15, https://doi.org/10.1007/s00382-025-07998-w, 2025.